Commun. Comput. Phys.
doi: 10.4208/cicp.181213.230514a

Vol. **17**, No. 1, pp. 146-188
January 2015

Numerical Simulation of Airfoil Vibrations Induced by Turbulent Flow

Miloslav Feistauer[1,2,*], Jaromír Horáček[2] and Petr Sváček[2,3]

[1] *Charles University in Prague, Faculty of Mathematics and Physics, Sokolovska 83, 186 75 Praha 8, Czech Republic.*
[2] *Institute of Thermomechanics, Academy of Sciences of the Czech Republic, Dolejškova 5, 182 00 Praha 8, Czech Republic.*
[3] *Czech Technical University Prague, Faculty of Mechanical Engineering, Karlovo nám. 13, 121 35 Praha 2, Czech Republic.*

Received 18 December 2013; Accepted (in revised version) 23 May 2014

Abstract. The subject of the paper is the numerical simulation of the interaction of two-dimensional incompressible viscous flow and a vibrating airfoil with large amplitudes. The airfoil with three degrees of freedom performs rotation around an elastic axis, oscillations in the vertical direction and rotation of a flap. The numerical simulation consists of the finite element solution of the Reynolds averaged Navier-Stokes equations combined with Spalart-Allmaras or $k-\omega$ turbulence models, coupled with a system of nonlinear ordinary differential equations describing the airfoil motion with consideration of large amplitudes. The time-dependent computational domain and approximation on a moving grid are treated by the Arbitrary Lagrangian-Eulerian formulation of the flow equations. Due to large values of the involved Reynolds numbers an application of a suitable stabilization of the finite element discretization is employed. The developed method is used for the computation of flow-induced oscillations of the airfoil near the flutter instability, when the displacements of the airfoil are large, up to ± 40 degrees in rotation. The paper contains the comparison of the numerical results obtained by both turbulence models.

AMS subject classifications: 74F10, 76D05, 76F60, 65N30

Key words: Fluid-structure interaction, flow induced vibrations, Reynolds averaged Navier-Stokes equations, turbulence models, finite element method, coupling algorithm.

1 Introduction

The interaction of flowing fluids and vibrating structures is the main subject of aeroelasticity, which studies the influence of aerodynamic forces on an elastic structure. The

*Corresponding author. *Email addresses:* feist@karlin.mff.cuni.cz (M. Feistauer), jaromirh@it.cas.cz (J. Horáček), svacek@marian.fsik.cvut.cz (P. Sváček)

flow-induced vibrations may affect negatively the operation and stability of aircrafts, blade machines, bridges, and many other structures in mechanical or civil engineering. The main goal of aero-elasticity is the prediction of the bounds of the structure stability, to cure the aero-elastic instabilities leading to flutter or divergence and to analyze post-critical regimes. This discipline is highly developed, particularly from engineering point of view (see, e.g., the monographs [10] and [34]).

From the point of view of mathematical theory, there are not too many works dealing with such problems, due to a high mathematical complexity of the problem, caused by the time-dependence of the domain occupied by the fluid and coupling of the system of equations describing flow and elastic structure. The mathematical simulation of fluid and structure interaction requires to consider viscous, usually turbulent flow, changes of the flow domain in time, nonlinear behaviour of the elastic structure and to solve simultaneously the evolution systems for the fluid flow and for the oscillating structure. Considering the Reynolds averaged Navier-Stokes equations and a vibrating structure with large displacements, the change of the fluid domain cannot be neglected. The methods with moving meshes [13, 25] must be employed and the application of efficient and robust methods for the numerical solution is required.

The subject of our attention is the numerical analysis of the interaction of viscous turbulent flow with a vibrating airfoil. Recent studies on numerical modelling of the postflutter behaviour of airfoils in laminar two-dimensional (2D) incompressible flow were overwieved by the authors in the previous study (Feistauer et al. [14]), where the method allowing the solution of large amplitude flow-induced vibrations of an airfoil with 3 degrees of freedom (3-DOF) was developed for laminar flow. However, none of the studies mentioned in this paper deals with turbulent flow, which is necessary to take into account for high Reynolds numbers ($10^5 - 10^8$).

For an extensive treatment of turbulent flows, one can be referred, e.g. to [27, 40, 42, 43, 46]. Turbulent flow has a three-dimensional character, but in a number of cases, two-dimensional models are applied to the numerical simulation of turbulent flow. Similar situation appears in theory, as can be found in [15]. In a turbulent flow simulation, techniques based on the Reynolds averaged Navier-Stokes (RANS) equations are often applied. As a result, the system called Reynolds equations (see [40, Chapter 4]) is obtained. It contains the so-called Reynolds stresses, evaluated with the aid of a turbulent viscosity model. It can be computed from algebraic relations or it can be obtained with the aid of the solution of additional equations for turbulence quantities, such as k and ω (see, e.g. [40, Chapter 10]).

The effect of turbulence in aeroelastic computations is studied in civil engineering as well as in turbomachine, nuclear and aerospace engineering applications. For example, Baxevanou et al. [2] modeled the aeroelastic stability of a wind turbine blade section. The Reynolds averaged Navier-Stokes equations for 2D incompressible flow were solved numerically using the finite volume method on structured, curvilinear grids using two versions of the $k-\omega$ high Reynolds number model of Wilcox with wall functions and wall treatment.

The response of suspension bridges to wind excitation was studied by Salvatori and Spinelli [41] by numerical simulations with a specifically developed finite element program implementing structural nonlinearities. The response under turbulent wind was evaluated through a Monte Carlo approach. The unsteady flow field around a 2D rectangular bridge section was studied by Mannini et al. [31], [32] using unsteady Reynolds-averaged Navier-Stokes (URANS) equations at Reynolds numbers from $2.6\cdot10^4$ to $1.8\cdot10^6$. The flow was simulated by the finite-volume unstructured solver and the results obtained with one- and two-equation turbulence models (Spalart-Allmaras, Wilcox $k-\omega$, Menter-SST, linearized explicit algebraic) were compared. A novel numerical algorithm for the study of the effects of wind turbulence on bridge flutter was proposed by Caracoglia [5]. The coupled-mode flutter threshold for bending-torsional modes of a long-span bridge is estimated in the time domain by stochastic calculus techniques.

Subcritical flutter characteristics were examined by Matsuzaki and Torii [33] using a bending-torsion wing model subjected to atmospheric turbulence with a view to applications for flutter boundary prediction. The wing response due to random inputs was represented by the autoregressive moving-average model. The effect of atmospheric turbulence on the flutter and post-flutter dynamics of a structurally nonlinear 2D airfoil in incompressible turbulent flow was investigated numerically by Poirel and Price [36], [38] using a Monte Carlo approach. A general overview of random flutter in aeroelasticity given by the random nature of a structure excitation in turbulent flow was published by Poirel and Price in the paper [37] concentrating on a numerical flutter investigation of 2D linear airfoil in turbulent flow.

Srinivasan et al. [45] used the finite difference method for the solution of 2D RANS equations modelling the turbulent flow around the oscillating airfoil NACA0015 with prescribed rotation, i.e., without any fluid-structure interaction. By testing five models of turbulence the authors found that one-equation models provide significant improvement over the algebraic and half-equation models but have their own limitation. A dynamically shaped rigid airfoil utilizing a moving flap has been studied by Lian et al. [26] at a Reynolds number of about 80 000, when the movement of the solid structure was prescribed. The RANS equations for incompressible fluids and two different versions of the $k-\varepsilon$ turbulence model have been employed. A pressure-based numerical procedure was based on the finite volume method using the moving grid. The algebraic model of turbulence was applied to the numerical simulation of turbulent flow-induced vibrations of an airfoil with two degrees of freedom (2-DOF) by Dubcova et al. [11] and [12]. Random flutter of the 2-DOF airfoil with freeplay nonlinearity in pitch was investigated numerically by Zhao et al. [53], [54] for low, intermediate and high level of turbulence. Poirel et al. [39] studied the low amplitude self-sustained pitch airfoil oscillations in incompressible flow by 2D numerical simulations in the Reynolds number range from $5.0\cdot10^4$ to $1.5\cdot10^5$. Both laminar and URANS calculations using the SST $k-\omega$ model with a low-Reynolds-number correction have been performed using commercial codes Gambit 2.3 and Fluent 6.3 and produced limit cycle pitching oscillations (LCO). It was shown that turbulence tends to suppress the pitching oscillations.

A 2-DOF airfoil moving in both pitching and plunging was studied numerically for transonic flow by Geissler [16] based on a 2D Navier-Stokes equations solver and the Spalart-Allmaras turbulence model. A numerical investigation of the 2-DOF bending/torsion flutter characteristics of an airfoil in 2D transonic flow was carried out by Weber et al. [51] using a time-domain method. The Reynolds averaged Navier-Stokes (RANS) equations were used and the turbulence modeling was based either on algebraic Baldwin-Lomax or one-equation Baldwin-Barth or Spalart-Allmaras turbulence models. The paper by Wang and Zha [50] investigates the NLR7301 airfoil limit cycle oscillation (LCO) in transonic flow caused by the flow nonlinearity of the fluid-structure interaction using detached eddy simulation (DES) of turbulence.

Everywhere, small amplitudes of structural vibrations were considered and no effects of large rotation amplitudes resulting in a nonlinear mass matrix for 3-DOF airfoil were taken into account as in previous authors study Feistauer et al. [14] for laminar flow. In the present paper we are concerned with numerical simulation of 2D viscous incompressible turbulent flow past a moving airfoil during flutter cycle oscillations. The airfoil is considered as a solid flexibly supported body with three degrees of freedom, allowing its vertical and torsional oscillations and the rotation of a flap. The turbulence is modelled by two models, namely by the one equation Spalart-Allmaras model [44] and also by the $k-\omega$ model [23,44].

From the above survey we can see that the Spalart-Allmaras and $k-\omega$ models are very popular in the simulation of turbulent flow. The Spalart-Allmaras model is based on one convection-diffusion-reaction equation only, which is its advantage in comparison to two-equation models as $k-\omega$ model. Moreover, the Spalart-Allmaras model is recommended to be applied to the simulation of turbulent flow around airfoils. On the other hand, the two-equation $k-\omega$ model offers more sophisticated (and, thus, more adequate) turbulence resolution. This is the reason that in our paper we consider both models and compare them from the point of view of their stability, accuracy and reliability.

The novelty of the paper consists in the development of a numerical method for the solution of the RANS equations in time-dependent domains, coupled with the system describing flow induced vibrations with large amplitudes of an airfoil with three degrees of freedom. We apply the finite element method in contrast to the above mentioned papers, where (except the works [11,12,14]) the flow is discretized by the finite difference or finite volume methods or even only commercial codes are used.

The time dependent computational domain and a moving grid are taken into account with the aid of the arbitrary Lagrangian-Eulerian (ALE) formulation. In order to avoid spurious numerical oscillations, the SUPG and div-div stabilization is applied. The solution of the ordinary differential equations is carried out by the Runge-Kutta method. Special attention is paid to the construction of the ALE mapping of a reference domain on the computational domain at individual time instants. The resulting nonlinear discrete algebraic systems are solved by the Oseen-like iterative processes. All components of the realization of the solution are assembled together by a coupling procedure. The algorithms of weak and strong coupling of flow and structure problems are formulated. The

method was tested on a flutter problem for which the stability boundary was computed by NASTRAN program code [28,29].

All details of the method are described here. The numerical tests prove that the developed method is sufficiently accurate and robust with respect to the Reynolds number. It allows the solution of FSI problems with large vibration amplitudes. Moreover, an important result is the comparison of the applicability of the Spalart-Allmaras and $k-\omega$ models of turbulence showing that the $k-\omega$ model appears to be more robust.

2 Description of the incompressible turbulent flow

We shall consider two-dimensional nonstationary flow of a viscous, incompressible fluid in a domain Ω_t depending on time $t \in [0,T]$, where $T > 0$. By $\overline{\Omega}_t$ and $\partial\Omega_t$ we shall denote the closure and the boundary, respectively, of the domain Ω_t. The boundary $\partial\Omega_t$ is the union of mutually disjoint parts Γ_D, Γ_O a Γ_{W_t}, i.e. $\partial\Omega_t = \Gamma_D \cup \Gamma_O \cup \Gamma_{W_t}$, where different boundary conditions are prescribed. The part Γ_D represents the inlet and fixed, impermeable walls, Γ_O denotes the outlet. We assume that Γ_D and Γ_O are independent of time in contrast to Γ_{W_t}, which is the moving airfoil boundary at time t. The moving airfoil surface Γ_{Wt} consists of two parts, the profile surface P_t and the flap surface F_t, i.e. $\Gamma_{W_t} = P_t \cup F_t$. We consider the flap separated from the main body of the airfoil by a narrow gap of a width g. See Fig. 1.

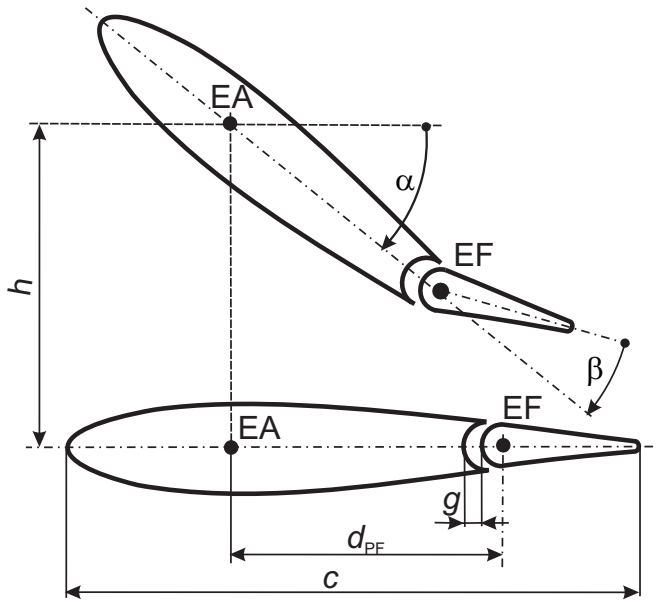

Figure 1: Model scheme – airfoil with 3 degrees of freedom with a gap.

2.1 Governing equations

Viscous incompressible flow is described by the velocity $\boldsymbol{u}=\boldsymbol{u}(x,t)$ and the kinematic pressure $p=p(x,t)$ depending on $x\in\overline{\Omega}_t$ and $t\in[0,T]$. The density of the fluid ρ is assumed to be constant. The character of the flow depends on the magnitude of the Reynolds number $Re=U_\infty c/\nu$, where ν is the kinematic viscosity, U_∞ denotes the far field velocity and c is the length of the airfoil chord. For a sufficiently small Reynolds number the flow is laminar. With the increasing value of the Reynolds number the flow becomes turbulent.

The turbulent flow is characterized by the fact that the fluid velocity field varies significantly and irregularly both in position and in time. The turbulence is a complicated motion, which results from the nonlinear advection that creates interactions between different scales of motion, which are the principal current (or the large eddies) and the eddying, random and reverse fluctuations. There are several strategies for the modelling of turbulent flow. For main concepts, see, e.g., the monographs [40, 46, 52].

One possibility is to use the Reynolds decomposition of the flow velocity $\boldsymbol{u}$ and the kinematic pressure p in the form

$$\begin{aligned}\boldsymbol{u}&=\overline{\boldsymbol{u}}+\boldsymbol{u}',\\ p&=\overline{p}+p',\end{aligned}\tag{2.1}$$

where $\overline{\boldsymbol{u}}$ is the mean part of the velocity vector, $\overline{p}$ is the mean part of the kinematic pressure, and $\boldsymbol{u}'$ and p' are their turbulent fluctuations. As a result we get the Reynolds averaged Navier-Stokes (RANS) equations [40, 52]

$$\begin{aligned}&\frac{\partial\overline{\boldsymbol{u}}}{\partial t}+(\overline{\boldsymbol{u}}\cdot\nabla)\overline{\boldsymbol{u}}+\nabla\overline{p}-\nabla\cdot\big(2(\nu+\nu_T)\overline{\mathbf{D}}\big)=0,\\ &\nabla\cdot\overline{\boldsymbol{u}}=0,\end{aligned}\qquad \text{in } \Omega_t,\tag{2.2}$$

where the components of the tensor $\overline{\mathbf{D}}$ are given by

$$\overline{D}_{ij}=\frac{1}{2}\left(\frac{\partial\overline{u_i}}{\partial x_j}+\frac{\partial\overline{u_j}}{\partial x_i}\right),\tag{2.3}$$

and the turbulent eddy viscosity coefficient $\nu_T=\nu_T(x,t)$ requires further modelling.

2.2 Reynolds averaged Navier-Stokes equations

In what follows, we shall work with the averaged velocity and pressure. Because of the simplification of notation, we shall omit the symbol "bar" and simply write $\boldsymbol{u}$ instead of $\overline{\boldsymbol{u}}$ and p instead of $\overline{p}$. This means that the above system will be written in the form

$$\begin{aligned}&\frac{\partial\boldsymbol{u}}{\partial t}+(\boldsymbol{u}\cdot\nabla)\,\boldsymbol{u}+\nabla p-\nabla\cdot\Big((\nu+\nu_T)(\nabla\boldsymbol{u}+\nabla^T\boldsymbol{u})\Big)=0,\\ &\nabla\cdot\boldsymbol{u}=0.\end{aligned}\tag{2.4}$$

System (2.4) is equipped with the initial condition

$$\boldsymbol{u}(x,0)=\boldsymbol{u}_0, \quad x\in\Omega_0, \tag{2.5}$$

and the boundary conditions

$$\begin{aligned}&\text{a) } \boldsymbol{u}|_{\Gamma_D}=\boldsymbol{u}_D, \qquad \text{b) } \boldsymbol{u}|_{\Gamma_{Wt}}=\boldsymbol{w}_D,\\ &\text{c) } -(p-p_{ref})n_i+(\nu+\nu_T)\sum_{j=1}^{2}\left(\frac{\partial u_i}{\partial x_j}+\frac{\partial u_j}{\partial x_i}\right)n_j=0 \quad \text{on } \Gamma_O, \quad i=1,2.\end{aligned} \tag{2.6}$$

Here $\boldsymbol{n}=(n_1,n_2)$ is the unit outer normal to the boundary $\partial\Omega_t$ of the domain Ω_t, $\boldsymbol{u}_D$ is a prescribed velocity on the part Γ_D. Condition (2.6) b) represents the assumption that the fluid adheres to the airfoil moving with the velocity $\boldsymbol{w}_D$. By p_{ref} we denote a prescribed reference (far field) pressure.

In numerical experiments carried out in Section 6, the initial and boundary data are specified as

$$\boldsymbol{u}_D=\boldsymbol{u}_0=(U_\infty,0), \tag{2.7}$$

where U_∞ denotes the magnitude of the far-field velocity. The vector function $\boldsymbol{w}_D$ denotes the velocity of the motion of the airfoil, which is a part of the sought solution.

In the above system (2.4), the averaged velocity $\boldsymbol{u}$, averaged pressure p and the turbulent viscosity ν_T are unknown functions. This system has to be completed by a turbulence model for ν_T. Here we shall use the Spalart-Allmaras and $k-\omega$ models.

2.3 Spalart-Allmaras one-equation turbulence model

This section is concerned with the description of the Spalart-Allmaras one-equation model [44] for the determination of the turbulent viscosity ν_T.

We introduce an auxiliary function $\widetilde{\nu}=\widetilde{\nu}(x,t)$, $x\in\overline{\Omega}_t$, $t\in[0,T]$, which is defined as a solution of the following initial-boundary value problem: Find $\widetilde{\nu}$ such that it satisfies the equation

$$\frac{\partial\widetilde{\nu}}{\partial t}+(\boldsymbol{u}\cdot\nabla)\widetilde{\nu}=\nabla\cdot(\varepsilon(\widetilde{\nu})\nabla\widetilde{\nu})+\frac{3}{2}c_{b_2}(\nabla\widetilde{\nu})^2+c_{b_1}\widetilde{S}(\widetilde{\nu})\widetilde{\nu}-s(\widetilde{\nu})\widetilde{\nu}^2, \tag{2.8}$$

in Ω_t, $t\in(0,T)$, the initial condition

$$\widetilde{\nu}(x,0)=\widetilde{\nu}^0(x) \quad \text{for } x\in\Omega_0, \tag{2.9}$$

and the boundary conditions

$$\widetilde{\nu}|_{\Gamma_D}=\widetilde{\nu}_D, \qquad \widetilde{\nu}|_{\Gamma_{Wt}}=0, \qquad \frac{\partial\widetilde{\nu}}{\partial n}\Big|_{\Gamma_O}=0. \tag{2.10}$$

The functions $\varepsilon(\widetilde{\nu})$, $\widetilde{S}(\widetilde{\nu})$, $s(\widetilde{\nu})$ are defined in such way that we successively set

$$\begin{aligned}
&\omega_{ij}=\frac{1}{2}\left(\frac{\partial u_i}{\partial x_j}-\frac{\partial u_j}{\partial x_i}\right),\ i,j=1,2, && S=\sqrt{2\sum_{i,j=2}^{2}\omega_{ij}^2},\\
&\varepsilon(\widetilde{\nu})=\frac{3}{2}(\nu+\widetilde{\nu}), && \chi(\widetilde{\nu})=\frac{\widetilde{\nu}}{\nu},\\
&f_{v_1}(\widetilde{\nu})=\frac{\chi^3(\widetilde{\nu})}{\chi^3(\widetilde{\nu})+c_v^3}, && f_{v_2}(\widetilde{\nu})=1-\frac{\chi(\widetilde{\nu})}{1+\chi(\widetilde{\nu})f_{v_1}(\widetilde{\nu})},\\
&\widetilde{S}(\widetilde{\nu})=\left(S+\frac{\widetilde{\nu}}{\kappa^2y^2}f_{v_2}(\widetilde{\nu})\right), && r(\widetilde{\nu})=\frac{\widetilde{\nu}}{\widetilde{S}(\widetilde{\nu})\kappa^2y^2},\\
&g(\widetilde{\nu})=r(\widetilde{\nu})+c_{w_2}(r^6(\widetilde{\nu})-r(\widetilde{\nu})), && s(\widetilde{\nu})=\frac{c_{w_1}}{y^2}\left(\frac{1+c_{w_3}^6}{1+\frac{c_{w_3}^6}{g^6(\widetilde{\nu})}}\right)^{\frac{1}{6}},
\end{aligned} \tag{2.11}$$

where $y=y(x)$ denotes the distance of a point $x\in\Omega_t$ from the nearest wall (e.g. airfoil surface, channel walls, etc.) The empirical constants appearing in the above formulas are taken from [52]:

$$\begin{aligned}
&c_{b_1}=0.1355, && c_{b_2}=0.622, && \beta=\frac{2}{3}, && c_v=7.1,\\
&c_{w_2}=0.3, && c_{w_3}=2.0, && \kappa=0.41,
\end{aligned} \tag{2.12}$$

and

$$c_{w_1}=\frac{c_{b_1}}{\kappa^2}+\frac{1+c_{b_2}}{\beta}. \tag{2.13}$$

Assuming that $\widetilde{\nu}$ is known, the turbulent viscosity ν_T used in (2.4) is defined by the relation

$$\nu_T=\widetilde{\nu}f_{v_1}(\widetilde{\nu}). \tag{2.14}$$

2.4 $k-\omega$ turbulence model

Another possibility is the application of two-equations turbulence models. Here $k-\omega$ turbulence model [23, 52] will be used. In this case the turbulent viscosity ν_T is defined by the relation

$$\nu_T=\frac{k}{\omega}, \tag{2.15}$$

where the functions $k=k(x,t)$ and $\omega=\omega(x,t)$ defined for $x\in\overline{\Omega}_t$, $t\in[0,T]$ are referred to as the turbulent kinetic energy and the specific turbulent dissipation rate, respectively.

They are obtained as solutions of the equations

$$\frac{\partial k}{\partial t}+(\boldsymbol{u}\cdot\nabla)k=P_k-\beta^*\omega k+\nabla\cdot((\nu+\sigma_k\nu_T)\nabla k), \tag{2.16}$$

$$\frac{\partial \omega}{\partial t}+(\boldsymbol{u}\cdot\nabla)\omega=P_\omega-\beta\omega^2+\nabla\cdot((\nu+\sigma_\omega\nu_T)\nabla\omega)+C_D, \tag{2.17}$$

equipped with the initial conditions

$$\begin{aligned} &k(x,0)=k_0(x),\\ &\omega(x,0)=\omega_0(x), \end{aligned} \qquad \text{for } x\in\Omega_0, \tag{2.18}$$

and the boundary conditions

$$\begin{aligned} &\text{a)}\quad k(x,t)=0, && \omega(x,t)=\omega_{wall}, && \text{for } x\in\Gamma_{Wt},\ t\in(0,T),\\ &\text{b)}\quad k(x,t)=k_D(x), && \omega(x,t)=\omega_D(x), && \text{for } x\in\Gamma_D,\ t\in(0,T),\\ &\text{c)}\quad \frac{\partial k}{\partial n}(x,t)=0, && \frac{\partial \omega}{\partial n}(x,t)=0, && \text{for } x\in\Gamma_O,\ t\in(0,T). \end{aligned} \tag{2.19}$$

The production terms are given by

$$\begin{aligned} &P_k=\frac{k}{\omega}\sum_{i,j=1}^{2}D_{ij}^2, \qquad P_\omega=\alpha_\omega\sum_{i,j=1}^{2}D_{ij}^2,\\ &C_D=\frac{\sigma_D}{\omega}\max\left\{\sum_{i=1}^{2}\frac{\partial k}{\partial x_i}\frac{\partial \omega}{\partial x_i},0\right\}. \end{aligned} \tag{2.20}$$

(The expressions D_{ij} are defined in a similar way as in (2.3).) The closure coefficients β, β^*, σ_k, σ_ω, α_ω are chosen by [23]:

$$\begin{aligned} &\beta=0.075, \quad \beta^*=0.09, \quad \sigma_\omega=0.5, \quad \sigma_k=\frac{2}{3}, \quad \kappa=0.41, \quad \sigma_D=0.5,\\ &\alpha_\omega=\frac{\beta}{\beta^*}-\sigma_\omega\frac{\kappa^2}{\beta^{*1/2}}. \end{aligned} \tag{2.21}$$

2.5 Specification of the initial and boundary conditions in turbulence models

In the Spalart-Allmaras model we choose

$$\tilde{\nu}_D=\tilde{\nu}^{(0)}=\tilde{\nu}, \tag{2.22}$$

where $\tilde{\nu}$ is chosen so that (cf. (2.14))

$$\tilde{\nu}f_{v_1}(\tilde{\nu}))=\nu/10. \tag{2.23}$$

As for the $k-\omega$ model, we set

$$\nu_T^0=\nu, \qquad k^0=\omega^0\nu, \qquad \omega^0=10\ \mathrm{s}^{-1}, \tag{2.24}$$

$$k_D=1.5\cdot 10^{-4}U_\infty^2, \qquad \omega_D=10\ \mathrm{s}^{-1}, \qquad \omega_{wall}=\frac{6\nu}{\beta y_1^2}, \tag{2.25}$$

where y_1 is the distance of the barycenter of the mesh element adjacent to the boundary used in the finite element method (see Section 4). This means that ω_{wall} depends on the mesh. The definition of ω_{wall} is motivated by the asymptotic behaviour of the specific dissipation rate ω close to the surface – see [52, Chapter 4].

2.6 Arbitrary Lagrangian-Eulerian method

In order to simulate flow in a moving domain Ω_t, we employ the arbitrary Lagrangian-Eulerian (ALE) method (cf. [35]), based on a regular one-to-one ALE mapping

$$\mathcal{A}_t:\overline{\Omega}_0\mapsto\overline{\Omega}_t, \quad Y\in\overline{\Omega}_0\mapsto x(Y,t)=\mathcal{A}_t(Y)\in\overline{\Omega}_t, \quad t\in[0,T]. \tag{2.26}$$

$\mathcal{A}_t$ is the identity in the part of the boundary $\partial\Omega_t$, where there is no interaction with the body and also there is no deformation of the boundary. The reference domain Ω_0 is identical with the domain occupied by the fluid at the initial time $t=0$. The coordinates of points $x\in\Omega_t$ are called the spatial coordinates, the coordinates of points $Y\in\Omega_0$ are called the ALE coordinates or the reference coordinates.

Now we define the domain velocity

$$\widetilde{\boldsymbol{w}}(Y,t)=\frac{\partial\mathcal{A}_t(Y)}{\partial t}=\frac{\partial x(Y,t)}{\partial t}. \tag{2.27}$$

This velocity can be expressed in the spatial coordinates as

$$\boldsymbol{w}(x,t)=\widetilde{\boldsymbol{w}}\left(\mathcal{A}_t^{-1}(x),t\right). \tag{2.28}$$

Further, for any function $f=f(x,t)$, $x\in\Omega_t$, $t\in[0,T]$ we set $\tilde{f}(Y,t)=f(\mathcal{A}_t(Y),t)$ and define its ALE derivative by

$$\frac{D^A}{Dt}f(x,t)=\frac{\partial\widetilde{f}}{\partial t}(Y,t), \qquad Y=\mathcal{A}_t^{-1}(x). \tag{2.29}$$

The application of the chain rule gives

$$\frac{D^A}{Dt}f=\frac{\partial f}{\partial t}+\boldsymbol{w}\cdot\nabla f. \tag{2.30}$$

2.7 Governing equations in the ALE form

Using relation (2.30), the Reynolds averaged Navier-Stokes equations and the turbulence models can be rewritten in the ALE form. First, the Reynolds averaged Navier-Stokes system reads

$$\frac{D^{\mathcal{A}}\boldsymbol{u}}{Dt}+((\boldsymbol{u}-\boldsymbol{w})\cdot\nabla)\,\boldsymbol{u}+\nabla p-\nabla\cdot\Big((\nu+\nu_T)(\nabla\boldsymbol{u}+\nabla\boldsymbol{u}^T)\Big)=0, \tag{2.31}$$

$$\nabla\cdot\boldsymbol{u}=0. \tag{2.32}$$

Further, the Spalart-Allmaras equation (2.8) has the ALE form

$$\frac{D^{\mathcal{A}}\widetilde{\nu}}{Dt}+((\boldsymbol{u}-\boldsymbol{w})\cdot\nabla)\widetilde{\nu}=\nabla\cdot(\varepsilon(\widetilde{\nu})\nabla\widetilde{\nu})+\frac{3}{2}c_{b_2}(\nabla\widetilde{\nu})^2+c_{b_1}\widetilde{S}(\widetilde{\nu})\widetilde{\nu}-s(\widetilde{\nu})\widetilde{\nu}^2, \tag{2.33}$$

and the $k-\omega$ turbulence model has the ALE form

$$\frac{D^{\mathcal{A}}k}{Dt}+((\boldsymbol{u}-\boldsymbol{w})\cdot\nabla)k=P_k-\beta^*\omega k+\nabla\cdot((\nu+\sigma_k\nu_T)\nabla k), \tag{2.34}$$

$$\frac{D^{\mathcal{A}}\omega}{Dt}+((\boldsymbol{u}-\boldsymbol{w})\cdot\nabla)\omega=P_\omega-\beta\omega^2+\nabla\cdot((\nu+\sigma_\omega\nu_T)\nabla\omega)+C_D. \tag{2.35}$$

3 Nonlinear equations of the airfoil motion

The deformation of the computational domain depends on the motion of the airfoil, which is described by the rotation angle $\alpha=\alpha(t)$ of the whole airfoil around an elastic axis EA, the rotation angle $\beta=\beta(t)$ of the flap around an elastic axis EF and the vertical displacement $h=h(t)$ of the whole airfoil, see Fig. 1. The functions $\alpha(t)$, $\beta(t)$ and $h(t)$ form a solution of the following system of nonlinear ordinary differential equations (see [20]):

$$\begin{aligned}
&m\ddot{h}+\big[(S_\alpha-S_\beta)\cos\alpha+S_\beta\cos(\alpha+\beta)\big]\,\ddot{\alpha}+S_\beta\ddot{\beta}\cos(\alpha+\beta)\\
&\quad-(S_\alpha-S_\beta)\dot{\alpha}^2\sin\alpha-S_\beta(\dot{\alpha}+\dot{\beta})^2\sin(\alpha+\beta)+D_{hh}\dot{h}+k_{hh}h=\mathcal{L},\\
&\big[(S_\alpha-S_\beta)\cos\alpha+S_\beta\cos(\alpha+\beta)\big]\,\ddot{h}+\big[(I_\alpha-2d_{PF}S_\beta)+2d_{PF}S_\beta\cos\beta\big]\,\ddot{\alpha}\\
&\quad+\big[I_\beta+d_{PF}S_\beta\cos\beta\big]\,\ddot{\beta}-d_{PF}S_\beta\dot{\beta}^2\sin\beta-2d_{PF}S_\beta\dot{\alpha}\dot{\beta}\sin\beta+D_{\alpha\alpha}\dot{\alpha}+k_{\alpha\alpha}\alpha=\mathcal{M}_\alpha,\\
&S_\beta\cos(\alpha+\beta)\ddot{h}+\big[I_\beta+d_{PF}S_\beta\cos\beta\big]\,\ddot{\alpha}+I_\beta\ddot{\beta}+d_{PF}S_\beta\dot{\alpha}^2\sin\beta+D_{\beta\beta}\dot{\beta}+k_{\beta\beta}\beta=\mathcal{M}_\beta.
\end{aligned} \tag{3.1}$$

Here $\mathcal{L}$ is the vertical component of the aerodynamical force acting on the whole airfoil, $\mathcal{M}_\alpha$ is the torsional moment of the aerodynamical force acting on the whole airfoil with respect to the axis EA, $\mathcal{M}_\beta$ is the torsional moment of the aerodynamical force acting on the flap of the airfoil with respect to the flap axis EF, D_{hh}, $D_{\alpha\alpha}$, $D_{\beta\beta}$ are the coefficients of a structural damping, S_α, I_α and m denote the static moment of the whole airfoil around

the elastic axis EA, the moment of inertia of the whole airfoil around the elastic axis EA and the mass of the whole profile, respectively, the coefficient S_β is the static moment of the flap of the airfoil around the flap axis EF and I_β is the moment of inertia of the flap of the airfoil around the flap axis EF. The constants k_{hh},$k_{\alpha\alpha}$,$k_{\beta\beta}$ denote the spring stiffness of the flexible support of the airfoil and d_{PF} is the distance between the elastic axis EA and the flap axis EF.

System (3.1) is equipped with the initial conditions

$$\begin{aligned} &\alpha(0)=\alpha_0, \qquad &&\dot{\alpha}(0)=\alpha_1, \\ &\beta(0)=\beta_0, \qquad &&\dot{\beta}(0)=\beta_1, \\ &h(0)=h_0, \qquad &&\dot{h}(0)=h_1. \end{aligned} \tag{3.2}$$

The interaction between the flow and the airfoil is given by the non-stationary force component $\mathcal{L}$ and the moments $\mathcal{M}_\alpha$ and $\mathcal{M}_\beta$ defined by

$$\mathcal{L}=-l\int_{P_t\cup F_t}\sum_{j=1}^{2}\tau_{2j}n_j\,\mathrm{d}S, \tag{3.3}$$

$$\mathcal{M}_\alpha=-l\int_{P_t\cup F_t}\sum_{i,j=1}^{2}\tau_{ij}n_j(-1)^i\left(x_{1+\delta_{1i}}-x^{EA}_{1+\delta_{1i}}\right)\mathrm{d}S, \tag{3.4}$$

$$\mathcal{M}_\beta=-l\int_{F_t}\sum_{i,j=1}^{2}\tau_{ij}n_j(-1)^i\left(x_{1+\delta_{1i}}-x^{EF}_{1+\delta_{1i}}\right)\mathrm{d}S, \tag{3.5}$$

where l is the depth of the segment of the airfoil, $\boldsymbol{n}=(n_1,n_2)$ is the outer unit normal to $\partial\Omega_t$ on $\Gamma_{Wt}=P_t\cup F_t$, the symbol δ_{ij} is the Kronecker symbol defined by $\delta_{ij}=1$ for $i=j$ and $\delta_{ij}=0$ for $i\neq j$, x_1 and x_2 are the coordinates of points on Γ_{Wt}, x_i^{EA}, $i=1,2$, are the coordinates of the current location of the elastic axis EA and x_i^{EF}, $i=1,2$, are the coordinates of the current location of the flap elastic axis EF. The stress tensor components are given by the relation

$$\tau_{ij}=\varrho\left[-p\delta_{ij}+(\nu+\nu_T)\left(\frac{\partial u_i}{\partial x_j}+\frac{\partial u_j}{\partial x_i}\right)\right]. \tag{3.6}$$

The interaction of the fluid and the airfoil is formed by the solution of the turbulent flow problem consisting of equations (2.31), (2.32) equipped with conditions (2.5), (2.6) and completed by the turbulence model (2.33), (2.9), (2.10) or (2.34), (2.35), (2.18), (2.19), which are coupled with the structural model (3.1), (3.2) via (3.3)-(3.6). In what follows, we shall be concerned with the discretization of the flow problem and describe the algorithm for the numerical solution of the complete fluid-structure interaction problem.

4 Discretization of the flow problem

4.1 Time discretization

In order to discretize the flow problem in time, we construct an equidistant partition of the time interval $[0,T]$ formed by time instants $0=t_0<t_1<\cdots<T$, $t_n=n\tau$, $n=0,1,\cdots$, with a time step $\tau>0$. We use the approximations $\boldsymbol{u}(t_n)\approx\boldsymbol{u}^n$, $p(t_n)\approx p^n$ and $\boldsymbol{w}(t_n)\approx\boldsymbol{w}^n$ at time t_n for the velocity, the pressure and the domain velocity, respectively. The ALE derivative will be approximated by the second-order backward difference formula (known as BDF2). For a given point $Y\in\Omega_0$ from the reference configuration on a given time level t_n we can write

$$\mathcal{A}_{t_{n-1}}(Y)=x_{n-1}\in\Omega_{t_{n-1}},\quad \mathcal{A}_{t_n}(Y)=x_n\in\Omega_{t_n},\quad \mathcal{A}_{t_{n+1}}(Y)=x_{n+1}\in\Omega_{t_{n+1}}. \tag{4.1}$$

Using definition (2.29), where we set $f:=\boldsymbol{u}$, we shall approximate the ALE derivative of the velocity at time t_{n+1} and point x_{n+1} by the formula

$$\begin{aligned}\frac{D^A\boldsymbol{u}}{Dt}(x_{n+1},t_{n+1})&\approx\frac{3\tilde{\boldsymbol{u}}^{n+1}(Y)-4\tilde{\boldsymbol{u}}^n(Y)+\tilde{\boldsymbol{u}}^{n-1}(Y)}{2\tau}\\&=\frac{3\boldsymbol{u}^{n+1}(x_{n+1})-4\boldsymbol{u}^n(x_n)+\boldsymbol{u}^{n-1}(x_{n-1})}{2\tau}.\end{aligned} \tag{4.2}$$

Taking into account that $\mathcal{A}_{t_{n+1}}(\mathcal{A}_{t_i}^{-1}(x_i))\in\Omega_{t_{n+1}}$, we introduce the functions $\widehat{\boldsymbol{u}}^i=\boldsymbol{u}^i\circ\mathcal{A}_{t_i}\circ\mathcal{A}_{t_{n+1}}^{-1}$, $i=n,n-1$, obtained by the transformation of $\boldsymbol{u}^n$ and $\boldsymbol{u}^{n-1}$ to the domain $\Omega:=\Omega_{t_{n+1}}$. Now the implicit scheme for the unknown functions $\boldsymbol{u}:=\boldsymbol{u}^{n+1}:\Omega\mapsto IR^2$ and $p:=p^{n+1}:\Omega\mapsto IR$ read

$$\frac{3\boldsymbol{u}-4\widehat{\boldsymbol{u}}^n+\widehat{\boldsymbol{u}}^{n-1}}{2\tau}+((\boldsymbol{u}-\boldsymbol{w}^{n+1})\cdot\nabla)\boldsymbol{u}+\nabla p-\nabla\cdot\Big((\nu+\nu_T)(\nabla\boldsymbol{u}+\nabla^T\boldsymbol{u})\Big)=0, \tag{4.3}$$

$$\nabla\cdot\boldsymbol{u}=0, \tag{4.4}$$

considered in Ω. We assume that $\boldsymbol{u}$ and p satisfy the boundary conditions (2.6).

Remark 4.1. In what follows, if we have a sequence $f^i:\Omega_{t_i}\to IR$, $i=0,1,\cdots$, and fix an index n, then we set $\widehat{f^i}=f^i\circ\mathcal{A}_{t_i}\circ\mathcal{A}_{t_{n+1}}^{-1}$, which are functions defined in $\Omega_{t_{n+1}}$.

4.2 Finite element space discretization of the RANS system

Let us assume that the approximation of the turbulent viscosity ν_T is known at time t_{n+1}. The starting point for the space discretization of system (4.3), (4.4) by the finite element method is the weak formulation. For simplicity we set $\Omega=\Omega_{t_{n+1}}$, $\Gamma_W=\Gamma_{Wt_{n+1}}$, $\boldsymbol{u}=\boldsymbol{u}^{n+1}$, $p=p^{n+1}$. We define the velocity and pressure function spaces

$$W=[H^1(\Omega)]^2,\qquad X=\{\boldsymbol{v}\in W;\boldsymbol{v}|_{\Gamma_D\cup\Gamma_W}=0\},\qquad Q=L^2(\Omega), \tag{4.5}$$

where $L^2(\Omega)$ is the Lebesgue space of square integrable functions over the domain Ω and $H^1(\Omega)$ is the Sobolev space of functions square integrable together with their first order derivatives. Further, if $\sigma \subset IR^2$, then by $(\cdot,\cdot)_\sigma$ we denote the scalar product in $L^2(\sigma)$: $(\varphi,\psi)_\sigma = \int_\sigma \varphi\psi \,\mathrm{d}x$. Moreover, by $\|\cdot\|_\sigma$ we shall denote the norm defined as $\|\varphi\|_\sigma = \max_\sigma |\varphi|$.

The weak formulation is obtained in a standard way. Eq. (4.3) is multiplied by a test function $\boldsymbol{v} \in X$ and Eq. (4.4) is multiplied by a test function $q \in Q$, integrated over the domain Ω, Green's theorem is applied, the boundary condition (2.6), c) is used and the resulting integral identities are summed. In this way we get the forms

$$\begin{aligned} a_{NS}(\nu_T,U^*,U,V) &= \frac{3}{2\tau}(\boldsymbol{u},\boldsymbol{v})_\Omega + \Big((\nu+\nu_T)(\nabla\boldsymbol{u}+\nabla^T\boldsymbol{u}),\nabla\boldsymbol{v}\Big)_\Omega \\ &\quad + \Big(((\boldsymbol{u}^*-\boldsymbol{w}^{n+1})\cdot\nabla)\boldsymbol{u},\boldsymbol{v}\Big)_\Omega - (p,\nabla\cdot\boldsymbol{v})_\Omega + (\nabla\cdot\boldsymbol{u},q)_\Omega, \\ f_{NS}(V) &= \frac{1}{2\tau}\Big(4\widehat{\boldsymbol{u}}^n - \widehat{\boldsymbol{u}}^{n-1},\boldsymbol{v}\Big)_\Omega - \int_{\Gamma_O} p_{ref}\boldsymbol{v}\cdot\boldsymbol{n}\,\mathrm{d}S, \end{aligned} \tag{4.6}$$

where we use the notation $U=(\boldsymbol{u},p)$, $U^*=(\boldsymbol{u}^*,p^*)$, $V=(\boldsymbol{v},q)$.

We define a *weak solution* as a couple $U=(\boldsymbol{u},p)\in W\times Q$ such that $\boldsymbol{u}$ satisfies the boundary conditions (2.6), a)-b), and the identity

$$a_{NS}(\nu_T,U,U,V) = f_{NS}(V) \quad \forall\, V=(\boldsymbol{v},q)\in X\times Q. \tag{4.7}$$

In order to apply the finite element method to the numerical solution, we assume that the domain Ω_Δ is a polygonal approximation of the computational domain at time t_{n+1}. By $\Gamma_{D\Delta}$ and $\Gamma_{W\Delta}$ we shall denote the parts of $\partial\Omega_\Delta$ approximating Γ_D and Γ_W, respectively. Further, by $\mathcal{T}_\Delta$ we denote a triangulation of Ω_Δ formed by a finite number of closed triangles. The parameter Δ denotes the maximal size of elements $K\in\mathcal{T}_\Delta$. We assume that any two different triangles are either disjoint or intersect each other in a common face or in a common vertex (cf., e.g. [6]). We use the Taylor-Hood P^2/P^1 elements [48]. This means that

$$\begin{aligned} Q_\Delta &= \{q\in C(\overline{\Omega}_\Delta); q|_K \in P^1(K)\ \forall K\in\mathcal{T}_\Delta\}, \\ W_\Delta &= \{\boldsymbol{v}\in [C(\overline{\Omega}_\Delta)]^2; \boldsymbol{v}|_K \in [P^2(K)]^2\ \forall K\in\mathcal{T}_\Delta\}, \\ X_\Delta &= \{\boldsymbol{v}\in W_\Delta; \boldsymbol{v}|_{\Gamma_{D\Delta}\cup\Gamma_{W\Delta}} = 0\}. \end{aligned} \tag{4.8}$$

Here the symbol $P^k(K)$ denotes the space of all polynomials on K of degree $\le k$. The couple (X_Δ,Q_Δ) satisfies the Babuška-Brezzi condition (see, e.g. [3,4,49]), which is important for the stability of the finite element scheme. The domain velocity $\boldsymbol{w}^{n+1}$ at time t_{n+1} is approximated by a function $\boldsymbol{w}_\Delta = \boldsymbol{w}_\Delta^{n+1}$, we use the approximations $\hat{\boldsymbol{u}}^i \approx \hat{\boldsymbol{u}}^i_\Delta$, $i=n,n-1$. Further, the forms a_{NS} and f_{NS} will be modified so that in (4.6) we shall write Ω_Δ instead of Ω.

Now the *approximate solution of the flow problem* is defined as a couple $U_\Delta=(\boldsymbol{u}_\Delta,p_\Delta)\in W_\Delta\times Q_\Delta$ such that

$$a_{NS}(\nu_T,U_\Delta,U_\Delta,V_\Delta) = f_{NS}(V_\Delta), \quad \forall V_\Delta=(\boldsymbol{v}_\Delta,q_\Delta)\in X_\Delta\times Q_\Delta, \tag{4.9}$$

and $\boldsymbol{u}_\Delta$ satisfies approximately the Dirichlet boundary conditions (2.6), a), b). This means that these conditions are satisfied at the *nodes*, i.e., the vertices and midpoints of sides of elements lying on the approximations $\Gamma_{D\Delta}$ and $\Gamma_{W\Delta}$ of Γ_D and Γ_W, respectively.

By the symbol $Re = U_\infty c/\nu$ we denote the Reynolds number. Here U_∞ denotes the magnitude of the far-field velocity and c is the length of the airfoil chord. For high Reynolds numbers approximate solutions can contain nonphysical spurious oscillations. In order to avoid them, we shall apply the streamline-diffusion (also called the SUPG – streamline upwind Petrov-Galerkin) stabilization and the div-div stabilization. For a velocity vector $\boldsymbol{u}^*$ we introduce the transport velocity $\overline{\boldsymbol{w}}^* = \overline{\boldsymbol{w}}^*(\boldsymbol{u}^*) = \boldsymbol{u}^* - \boldsymbol{w}_\Delta^{n+1}$ and define the forms

$$\begin{aligned}
\ell_{NS}(\nu_T, U^*, U, V) &= \sum_{K\in\mathcal{T}_\Delta} \delta_K \left(\frac{3}{2\tau}\boldsymbol{u} - \nabla\cdot((\nu+\nu_T)(\nabla\boldsymbol{u}+\nabla^T\boldsymbol{u})), \boldsymbol{v} \right)_K \\
&\quad + \sum_{K\in\mathcal{T}_\Delta} \delta_K((\overline{\boldsymbol{w}}^*\cdot\nabla)\boldsymbol{u} + \nabla p, (\overline{\boldsymbol{w}}\cdot\nabla)\boldsymbol{v})_K, \\
F_{NS}(V) &= \sum_{K\in\mathcal{T}_\Delta} \delta_K \left(\frac{1}{2\tau}(4\widehat{\boldsymbol{u}}^n - \widehat{\boldsymbol{u}}^{n-1}), (\overline{\boldsymbol{w}}\cdot\nabla)\boldsymbol{v} \right)_K, \\
P_{NS}(U, V) &= \sum_{K\in\mathcal{T}_\Delta} \tau_K(\nabla\cdot\boldsymbol{u}, \nabla\cdot\boldsymbol{v})_K.
\end{aligned} \tag{4.10}$$

Here

$$U = (\boldsymbol{u}, p), \qquad U^* = (\boldsymbol{u}^*, p), \qquad V = (\boldsymbol{v}, q),$$

and $\delta_K, \tau_K \geq 0$ are parameters defined on the basis of results from [17] and [30] and our numerical experiments and tests. We put

$$\delta_K = \delta^* \frac{h_K}{2\|\overline{\boldsymbol{w}}^*\|_K} \xi(\Re_K^{\overline{\boldsymbol{w}}^*}), \tag{4.11}$$

where $\|\overline{\boldsymbol{w}}^*\|_K = \max_K |\overline{\boldsymbol{w}}^*|$, h_K is the size of K measured in the direction of $\overline{\boldsymbol{w}}^*$ and

$$\Re_K^{\overline{\boldsymbol{w}}^*} = \frac{h_K\|\overline{\boldsymbol{w}}^*\|_K}{2\nu}, \qquad \xi(\Re_K^{\overline{\boldsymbol{w}}^*}) = \min\left(\frac{\Re_K^{\overline{\boldsymbol{w}}^*}}{6}, 1 \right). \tag{4.12}$$

The parameters τ_K are defined by

$$\tau_K = \tau^* h_K \|\overline{\boldsymbol{w}}^*\|_K, \quad \tau^* \in (0,1]. \tag{4.13}$$

In practical computations we use the values $\delta^* = 0.025$ and $\tau^* = 1$.

The solution of the stabilized discrete problem is such a couple $U_\Delta = (\boldsymbol{u}_\Delta, p_\Delta) \in W_\Delta \times Q_\Delta$ that $\boldsymbol{u}_\Delta$ satisfies the boundary conditions (2.6), a), b) at the nodes lying on $\Gamma_{D\Delta} \cup \Gamma_W$ and

$$\begin{aligned}
&a_{NS}(\nu_T, U_\Delta, U_\Delta, V_\Delta) + \ell_{NS}(\nu_T, U_\Delta, U_\Delta, V_\Delta) + P_{NS}(U_\Delta, V_\Delta) \\
&= f_{NS}(V_\Delta) + F_{NS}(V_\Delta), \qquad \forall V_\Delta = (\boldsymbol{v}_\Delta, q_\Delta) \in X_\Delta \times Q_\Delta.
\end{aligned} \tag{4.14}$$

The couple $(\boldsymbol{u}_\Delta, p_\Delta)$ represents the approximate solution on the time level t_{n+1} defined in the approximation of the domain $\Omega_{t_{n+1}}$.

Remark 4.2. The above procedure can also be used for the numerical solution of laminar flow. We simply set $\nu_T = 0$ and solve problem (4.14). To this end, the following Oseen iterative process can be used. Starting from an initial approximation $U_{\Delta,0}^{n+1}$ at time t_{n+1} and assuming that the iteration $U_{\Delta,m}^{n+1}$ has already been computed, we define $U_{\Delta,m+1}^{n+1} = (\boldsymbol{u}_{\Delta,m+1}, p_{\Delta,m+1}) \in W_\Delta \times Q_\Delta$ satisfying (2.6), a), b) at the nodes on $\Gamma_{D\Delta} \cup \Gamma_{W\Delta}$ and

$$\begin{aligned} &a_{NS}(0, U_{\Delta,m}^{n+1}, U_{\Delta,m+1}^{n+1}, V_\Delta) + \ell_{NS}(0, U_{\Delta,m}^{n+1}, U_{\Delta,m+1}^{n+1}, V_\Delta) + P_{NS}(U_{\Delta,m+1}^{n+1}, V_\Delta) \\ &= f_{NS}(V_\Delta) + F_{NS}(V_\Delta), \qquad \forall V_\Delta = (\boldsymbol{v}_\Delta, q_\Delta) \in X_\Delta \times Q_\Delta. \end{aligned} \tag{4.15}$$

We obtain a sequence $U_{\Delta,m}^{n+1}$, $m = 0,1,\cdots$, and assume that it converges to the solution U_Δ^{n+1} of Eq. (4.14) with $\nu_T = 0$. We set $U_{\Delta,0}^1 = (\boldsymbol{u}_\Delta^0, \overline{p})$ and for each time level t_{n+1}, $n \geq 1$, we set $U_{\Delta,0}^{n+1} = (2\widehat{\boldsymbol{u}}_\Delta^n - \widehat{\boldsymbol{u}}_\Delta^{n-1}, p_\Delta^n)$. The numerical realization of the Oseen iterations is described e.g. in [14].

4.3 Discretization of the Spalart-Allmaras turbulence equation

Eq. (2.33) is discretized in time similarly as the RANS system (2.31)-(2.32) by the second-order backward difference formula. At every time t_k we approximate $\widetilde{\nu}(t_k) \approx \widetilde{\nu}^k$. Let us assume that we have already obtained the approximations $\boldsymbol{u}^n$ and $\tilde{\nu}^n$. Then, as in Remark 4.1, we set

$$\widehat{\widetilde{\nu}}^{n-1} = \widetilde{\nu}^{n-1} \circ \mathcal{A}_{t_{n-1}} \circ \mathcal{A}_{t_{n+1}}^{-1}, \qquad \widehat{\widetilde{\nu}}^{n} = \widetilde{\nu}^{n} \circ \mathcal{A}_{t_{n}} \circ \mathcal{A}_{t_{n+1}}^{-1}, \tag{4.16}$$

which is the transformation of the functions $\tilde{\nu}^{n-1}$, $\tilde{\nu}^n$ from the domains $\Omega_{t_{n-1}}$, Ω_{t_n} to $\Omega_{t_{n+1}}$. For simplicity we shall use the notation ψ for the function $\tilde{\nu}^{(n+1)}$.

Because of computing the numerical solution of Eq. (2.33) at time t_{n+1} we shall use the following linearization of nonlinear terms:

$$\begin{aligned} &\varepsilon(\psi)\nabla\psi \approx \varepsilon(\widehat{\widetilde{\nu}}^n)\nabla\psi, \\ &(\nabla\psi)^2 \approx \nabla\widehat{\widetilde{\nu}}^n \cdot \nabla\psi, \\ &s(\psi)\psi^2 \approx s(\widehat{\widetilde{\nu}}^n)\left[(\widehat{\widetilde{\nu}}^n)^2 + 2\widehat{\widetilde{\nu}}^n(\psi - \widehat{\widetilde{\nu}}^n)\right] = s(\widehat{\widetilde{\nu}}^n)(2\widehat{\widetilde{\nu}}^n\psi - (\widehat{\widetilde{\nu}}^n)^2), \\ &\widetilde{S}(\psi)\psi \approx \widetilde{S}(\widehat{\widetilde{\nu}}^n)\widehat{\widetilde{\nu}}^n. \end{aligned} \tag{4.17}$$

The error of this linearization is of order $\mathcal{O}(\tau)$ (similarly in (4.49)). Nevertheless, it appears that the changes in other terms are larger, because in FSI simulations, the time step must be sufficiently small. If there is a need to increase the accuracy, it is possible to apply a simple iterative process. However, our numerical experiments showed that at most one iteration was necessary. On the basis of (4.17) we obtain the following linearized scheme

for the computation of the function ψ:

$$\begin{aligned}&\frac{3\psi-4\widehat{\widetilde{\nu}}^n+\widehat{\widetilde{\nu}}^{n-1}}{2\Delta t}+(\boldsymbol{u}-\boldsymbol{w})\cdot\nabla\psi\\&=\mathrm{div}(\varepsilon(\widehat{\widetilde{\nu}}^n)\nabla\psi)+\frac{3}{2}c_{b_2}\nabla\widehat{\widetilde{\nu}}^n\cdot\nabla\psi+c_{b_1}\widetilde{S}(\widehat{\widetilde{\nu}}^n)\widehat{\widetilde{\nu}}^n-s(\widehat{\widetilde{\nu}}^n)(2\widehat{\widetilde{\nu}}^n\psi-(\widehat{\widetilde{\nu}}^n)^2),\quad n=0,1,\cdots,\end{aligned}\tag{4.18}$$

which is equipped with the boundary conditions (2.10), rewritten now for the function ψ:

$$\psi|_{\Gamma_D}=\tilde{\nu}_D,\qquad \psi|_{\Gamma_W}=0,\qquad \frac{\partial\psi}{\partial n}\Big|_{\Gamma_O}=0.\tag{4.19}$$

The space discretization of problem (4.18)-(4.19) is carried out by the finite element method over the triangulation $\mathcal{T}_\Delta$ of the domain Ω_Δ, which is a polygonal approximation of the domain $\Omega_{t_{n+1}}$. We define the spaces

$$\mathcal{V}_\Delta=\left\{\varphi\in C(\overline{\Omega}_\Delta);\ \varphi|_K\in P_1(K)\ \forall K\in\mathcal{T}_\Delta\right\},\tag{4.20}$$

$$\mathcal{V}_\Delta^0=\{\varphi\in\mathcal{V}_\Delta;\ \varphi=0\text{ on }\Gamma_{D\Delta}\cup\Gamma_{W\Delta}\},\tag{4.21}$$

and the forms

$$\begin{aligned}B^{sa}(\boldsymbol{u},\psi,\varphi)=&\frac{3}{2\Delta t}(\psi,\varphi)_{\Omega_\Delta}+(\varepsilon(\widehat{\widetilde{\nu}}^n)\nabla\psi,\nabla\varphi)_{\Omega_\Delta}\\&+((\boldsymbol{u}-\boldsymbol{w})\cdot\nabla\psi,\varphi)_{\Omega_\Delta}-\left(\frac{3}{2}c_{b_2}\nabla\widehat{\widetilde{\nu}}^n\cdot\nabla\psi-2s(\widehat{\widetilde{\nu}}^n)\widehat{\widetilde{\nu}}^n\psi,\varphi\right)_{\Omega_\Delta},\end{aligned}\tag{4.22}$$

$$L^{sa}(\varphi)=\frac{1}{2\Delta t}(2\widehat{\widetilde{\nu}}^n-\widehat{\widetilde{\nu}}^{n-1},\varphi)_{\Omega_\Delta}+(c_{b_1}\widetilde{S}(\widehat{\widetilde{\nu}}^n)\widehat{\widetilde{\nu}}^n+s(\widehat{\widetilde{\nu}}^n)(\widehat{\widetilde{\nu}}^n)^2,\varphi)_{\Omega_\Delta}.\tag{4.23}$$

Assuming that $\boldsymbol{u}$ is known, the approximate solution of problem (4.18), (4.19) is defined as a function $\psi_\Delta\in\mathcal{V}_\Delta$ satisfying the Dirichlet boundary conditions (4.19) at the vertices lying on $\Gamma_{D\Delta}\cup\Gamma_{W\Delta}$ such that

$$B^{sa}(\boldsymbol{u},\psi_\Delta,\varphi_\Delta)=L^{sa}(\varphi_\Delta),\quad\forall\varphi_\Delta\in\mathcal{V}_\Delta^0.\tag{4.24}$$

In the case of large Reynolds numbers, we apply the SUPG stabilization, combined with discontinuity capturing (DC) introducing an additional dissipation in the crosswind direction. (See, e.g., [21] and [7].) To this end, we define the vector-valued function

$$\boldsymbol{b}=\boldsymbol{b}(\boldsymbol{u})=\boldsymbol{u}-\boldsymbol{w}_\Delta^{n+1}-\frac{3}{2}c_{b_2}\nabla\widehat{\widetilde{\nu}}^n.\tag{4.25}$$

By ψ^* we denote an auxiliary variable (approximation of ψ) and introduce the forms

$$B^{sa}_{SUPG}(\boldsymbol{u},\psi,\varphi)=\sum_{K\in\mathcal{T}_\Delta}\tilde{\delta}_K\left(\frac{3\psi}{2\Delta t}+\boldsymbol{b}\cdot\nabla\psi-\mathrm{div}(\varepsilon(\widetilde{\nu}^n)\nabla\psi)+2s(\widetilde{\nu}^n)\widetilde{\nu}^n\psi,\boldsymbol{b}\cdot\nabla\varphi\right)_K, \tag{4.26}$$

$$L^{sa}_{SUPG}(\boldsymbol{u},\varphi)=\sum_{K\in\mathcal{T}_\Delta}\widetilde{\delta}_K\left(\frac{4\widetilde{\nu}^n-\widetilde{\nu}^{n-1}}{2\Delta t}+c_{b_1}\widetilde{S}(\widetilde{\nu}^n)\widetilde{\nu}^n+s(\widetilde{\nu}^n)(\widetilde{\nu}^n)^2,\boldsymbol{b}\cdot\nabla\varphi\right)_K, \tag{4.27}$$

$$\begin{aligned}B^{sa}_{DC}(\boldsymbol{u},\psi^*,\psi,\varphi)=&\sum_{K\in\mathcal{T}_\Delta}\alpha_K(\psi^*)(\nabla\psi,\nabla\varphi)_K\\&+\sum_{K\in\mathcal{T}_\Delta}\left((\max(\alpha_K(\psi^*)-\alpha'_K,0)-\alpha_K(\psi^*))\frac{\boldsymbol{b}\otimes\boldsymbol{b}}{\|\boldsymbol{b}\|^2_K}\nabla\psi,\nabla\varphi\right)_K.\end{aligned} \tag{4.28}$$

Here

$$\widetilde{\delta_K}=\left(\frac{4\|\varepsilon(\widetilde{\nu}^n)\|_K}{h_K^2}+\frac{2\|\boldsymbol{b}\|_K}{h_K}+\|s(\widetilde{\nu}^n)\|_K\right)^{-1}, \tag{4.29}$$

$$\boldsymbol{b}\otimes\boldsymbol{b}=\begin{pmatrix}b_1^2, & b_1b_2\\ b_1b_2, & b_2^2\end{pmatrix} \tag{4.30}$$

and

$$\alpha'_K=\widetilde{\delta}_K\|\boldsymbol{b}\|^2_K. \tag{4.31}$$

The norm $\|\boldsymbol{b}\|^2_K$ is defined by

$$\|\boldsymbol{b}\|_K=\max_K(|b_1|+|b_2|). \tag{4.32}$$

Similarly we define the norms $\|\varepsilon(\widetilde{\nu}^n)\|_K$ and $\|s(\widetilde{\nu}^n)\|_K$.

Further, we define the local element residuals

$$\begin{aligned}\mathrm{res}_K(\psi^*)=&\frac{3\psi^*-4\widetilde{\nu}^n+\widetilde{\nu}^{n-1}}{2\Delta t}+\boldsymbol{b}\cdot\nabla\psi^*-\mathrm{div}(\varepsilon(\widetilde{\nu}^n)\nabla\psi^*)-s(\widetilde{\nu}^n)(\widetilde{\nu}^n)^2\\&-c_{b_1}\widetilde{S}(\widetilde{\nu}^n)+2s(\widetilde{\nu}^n)\widetilde{\nu}^n\psi^*,\end{aligned} \tag{4.33}$$

and set

$$\alpha_K(\psi^*)=\begin{cases}\dfrac{1}{2}A_K(\psi^*)h_K\dfrac{\|\mathrm{res}_K(\psi^*)\|_K}{\|\nabla\psi^*\|_K} & \text{if } \|\nabla\psi^*\|_K\neq 0,\\ 0 & \text{elsewhere,}\end{cases} \tag{4.34}$$

where h_K is the characteristics length of the element K (we use the size of the element K measured in the direction of $\boldsymbol{b}$), A_K is given by

$$A_K(\psi^*)=\max\left(0,\,0.7-\frac{2\varepsilon(\widetilde{\nu}^n)}{\|a_1(\psi^*)\|_Kh_K}\right) \tag{4.35}$$

with

$$a_1(\psi^*)=\frac{\mathrm{res}_K(\psi^*)}{\|\nabla\psi^*\|_K}\,. \tag{4.36}$$

Now let us define the complete stabilized Spalart-Allmaras turbulence model forms

$$B^{sa}_{TM}(\boldsymbol{u},\psi^*,\psi,\varphi)=B^{sa}(\boldsymbol{u},\psi,\varphi)+B^{sa}_{SUPG}(\boldsymbol{u},\psi,\varphi)+B^{sa}_{DC}(\boldsymbol{u},\psi^*,\psi,\varphi), \tag{4.37}$$

$$L^{sa}_{TM}(\boldsymbol{u}_\Delta,\varphi)=L^{sa}(\varphi)+L^{sa}_{SUPG}(\boldsymbol{u},\varphi). \tag{4.38}$$

Then (provided the finite element approximation $\boldsymbol{u}_\Delta$ of the flow velocity at time t_{n+1} is given), the stabilized discrete problem for ψ is formulated in the following way: Find $\psi_\Delta\in\mathcal{V}_\Delta$ satisfying the Dirichlet boundary conditions (4.19) at the vertices lying on $\Gamma_{D\Delta}\cup\Gamma_{W\Delta}$ such that

$$B^{sa}_{TM}(\boldsymbol{u},\psi_\Delta,\psi_\Delta,\varphi_\Delta)=L^{sa}_{TM}(\boldsymbol{u},\varphi_\Delta)\quad\forall\varphi_\Delta\in\mathcal{V}^0_\Delta. \tag{4.39}$$

4.3.1 The solution of the complete Spalart-Allmaras turbulent flow problem

Summarizing (4.10), (2.14) and (4.39), we can formulate the scheme for the computation of turbulent flow at the time instant t_{n+1} in the polygonal approximation Ω_Δ of the domain $\Omega_{t_{n+1}}$: Find $U_\Delta=(\boldsymbol{u}_\Delta,p_\Delta)$, ψ_Δ, $\widetilde{\nu}_\Delta$, ν_{T_Δ} such that

a) $U_\Delta=(\boldsymbol{u}_\Delta,p_\Delta)\in W_\Delta\times Q_\Delta$,
$\boldsymbol{u}_\Delta$ satisfies (2.6), a), b) at the nodes lying on $\Gamma_{D\Delta}$ and $\Gamma_{W\Delta}$,
$a_{NS}(\nu_{T\Delta},U_\Delta,U_\Delta,V_\Delta)+\ell_{NS}(\nu_{T\Delta},U_\Delta,U_\Delta,V_\Delta)+P_{NS}(U_\Delta,V_\Delta)$
$=f_{NS}(V_\Delta)+F_{NS}(V_\Delta)\quad\forall V_\Delta\in X_\Delta\times Q_\Delta$,

b) $\psi_\Delta\in\mathcal{V}_\Delta$,
$B^{sa}_{TM}(\boldsymbol{u}_\Delta,\psi_\Delta,\psi_\Delta,\varphi_\Delta)=L^{sa}_{TM}(\boldsymbol{u}_\Delta,\varphi_\Delta)\quad\forall\varphi_\Delta\in\mathcal{V}^0_\Delta$,

c) $\widetilde{\nu}_\Delta=\psi_\Delta$,

d) $\nu_{T\Delta}=\widetilde{\nu}_\Delta f_{v_1}(\widetilde{\nu}_\Delta)$. (4.40)

If we obtain the solution of this problem, then $(\boldsymbol{u}^{n+1}_\Delta,p^{n+1}_\Delta)=(\boldsymbol{u}_\Delta,p_\Delta)$, $\widetilde{\nu}^{(n+1)}_\Delta=\widetilde{\nu}_\Delta=\psi_\Delta$ and $\nu^{(n+1)}_{T\Delta}=\nu_{T\Delta}$ represent the approximate solution of the Spalart-Allmaras turbulence model at time t_{n+1}. The solution of problem (4.40) is carried out with the use of the following Oseen-like iterative process.

4.3.2 Algorithm for the solution of the discrete Spalart-Allmaras turbulent flow problem at time t_{n+1}

(0) In the beginning of the time marching process set $n=0$, $U^{-1}_\Delta=U^0_\Delta=(\boldsymbol{u}^0,p_{ref})$, $\widetilde{\nu}^{(-1)}_\Delta=\widetilde{\nu}^{(0)}_\Delta=\widetilde{\nu}_\Delta$, where $\widetilde{\nu}_\Delta$ is chosen so that $\widetilde{\nu}_\Delta f_{v_1}(\widetilde{\nu}_\Delta)=\nu/10$ (see the conditions specified in (2.7) and Section 2.5). Then find $\psi^*_\Delta\in\mathcal{V}_\Delta$ satisfying the Dirichlet boundary conditions (4.19) at the vertices lying on $\Gamma_{D\Delta}\cup\Gamma_{W\Delta}$ and

$$B^{sa}(\boldsymbol{u}^0,\psi^*_\Delta,\varphi_\Delta)+B^{sa}_{SUPG}(\boldsymbol{u}^0,\psi^*_\Delta,\varphi_\Delta)=L^{sa}_{TM}(\boldsymbol{u}^0,\varphi_\Delta)\quad\forall\varphi_\Delta\in\mathcal{V}^0_\Delta. \tag{4.41}$$

(In this way we get the initial value of ψ_Δ^*.)

(1) Let $\varepsilon>0$ be given. Let the approximation Ω_Δ of the domain $\Omega_{t_{n+1}}$ and $\boldsymbol{w}_\Delta^{n+1}$, $\widehat{u}_\Delta^{n-1}$, $\widehat{u}_\Delta^n$, $\widehat{\widetilde{\nu}}_\Delta^{n-1}$, $\widehat{\widetilde{\nu}}_\Delta^n$, $\widehat{\nu}_{T\Delta}$ (quantities transformed to the approximation of the domain $\Omega_{\Delta t_{n+1}}$ by Remark 4.1) have already been determined. Set

$$\nu_\Delta^*:=\widehat{\nu}_{T\Delta}^n, \qquad \psi_\Delta^*:=\widehat{\widetilde{\nu}}_\Delta^n, \qquad U_\Delta^*:=(\widehat{\boldsymbol{u}}_\Delta^n,\widehat{p}_\Delta^n). \tag{4.42}$$

(2) Find $U_\Delta=(\boldsymbol{u}_\Delta,p_\Delta)\in W_\Delta\times Q_\Delta$ such that $\boldsymbol{u}_\Delta$ satisfies the boundary conditions (2.6) at the nodes on $\Gamma_{D\Delta}\cup\Gamma_{W\Delta}$ and

$$\begin{aligned}&a_{NS}(\nu_{T\Delta}^*,U_\Delta^*,U_\Delta,V_\Delta)+\ell_{NS}(\nu_{T\Delta}^*,U_\Delta^*,U_\Delta,V_\Delta)+P_{NS}(U_\Delta,V_\Delta)\\ &=f_{NS}(V_\Delta)+F_{NS}(V_\Delta) \qquad \forall V_\Delta\in X_\Delta\times Q_\Delta.\end{aligned} \tag{4.43}$$

(3) Find $\psi_\Delta\in\mathcal{V}_\Delta$ such that it satisfies the Dirichlet conditions (4.19) at the vertices on $\Gamma_{D\Delta}\cup\Gamma_{W\Delta}$ and

$$B_{TM}^{sa}(\boldsymbol{u}_\Delta,\psi_\Delta^*,\psi_\Delta,\varphi_\Delta)=L_{TM}^{sa}(\boldsymbol{u}_\Delta,\varphi_\Delta) \qquad \forall\varphi_\Delta\in\mathcal{V}_\Delta^0. \tag{4.44}$$

(4) Set $\widetilde{\nu}_\Delta:=\psi_\Delta$, $\nu_{T\Delta}:=\widetilde{\nu}_\Delta f_{v_1}(\widetilde{\nu}_\Delta)$.

(5) If

$$\|\nu_{T\Delta}^*-\nu_{T\Delta}\|<\varepsilon \quad\text{and}\quad \|U_\Delta^*-U_\Delta\|<\varepsilon, \tag{4.45}$$

then set

$$U_\Delta^{(n+1)}:=U_\Delta, \qquad \widetilde{\nu}_\Delta^{(n+1)}:=\psi_\Delta, \qquad \nu_{T\Delta}^{(n+1)}:=\nu_{T\Delta}, \tag{4.46}$$

else

$$\nu_{T\Delta}^*:=\nu_{T\Delta}, \qquad U_\Delta^*:=U_\Delta, \qquad \psi_\Delta^*:=\psi_\Delta, \tag{4.47}$$

and go to (2).

Remark 4.3. In order to increase the stability of this algorithm, it is suitable to apply a few inner iterations in (4.44) of the following form: Set $\psi_{\Delta,0}:=\psi_\Delta^*$ and for $i=0,\cdots,l$ ($l=1$ or 2) find $\psi_{\Delta,i+1}\in\mathcal{V}_\Delta$ such that it satisfies the Dirichlet conditions (4.19) at the vertices from $\Gamma_{D\Delta}\cup\Gamma_{W\Delta}$ and

$$B_{TM}^{sa}(\boldsymbol{u}_\Delta,\psi_{\Delta,i},\psi_{\Delta,i+1},\varphi_\Delta)=L_{TM}^{sa}(\boldsymbol{u}_\Delta,\varphi_\Delta) \qquad \forall\varphi_\Delta\in\mathcal{V}_\Delta^0. \tag{4.48}$$

Then put $\psi_\Delta=\psi_{\Delta,l+1}$.

4.4 Discretization of the $k-\omega$ turbulence model

The discretization of the $k-\omega$ system (2.34), (2.35) is carried out in a similar way as in the previous section. The time derivative is approximated by the second-order backward difference formula, use suitable test functions φ_k and φ_ω for the obtained approximations for k and ω, respectively. Then we use the notation introduced in Remark 4.1 and introduce the following linearized approximations:

$$\begin{aligned}
&\beta^*\omega k(t_{n+1}) \approx 2\beta^*\widehat{\omega}^n k^{n+1} - \beta^*\widehat{\omega}^n\widehat{k}^n,\\
&\beta\omega^2(t_{n+1}) \approx 2\beta\widehat{\omega}^n\omega^{n+1} - \beta(\widehat{\omega}^n)^2,\\
&P_k(t_{n+1}) \approx \widehat{P_k(t_n)}, \qquad P_\omega(t_{n+1}) \approx \widehat{P_\omega(t_n)}.
\end{aligned} \tag{4.49}$$

Further, we use the notation

$$\begin{aligned}
&\varepsilon_k = \nu + \sigma_k\widehat{\nu}_T^n, \qquad \varepsilon_\omega = \nu + \sigma_\omega\widehat{\nu}_T^n, \qquad \Lambda^* = (k^*,\omega^*),\\
&\Lambda = (k,\omega), \qquad \Phi = (\varphi_k,\varphi_\omega), \qquad \overline{\boldsymbol{w}} = \overline{\boldsymbol{w}}(\boldsymbol{u}) = \boldsymbol{u} - \boldsymbol{w}_\Delta^{n+1}.
\end{aligned} \tag{4.50}$$

Then we get the following forms:

$$\begin{aligned}
B^{k\omega}(\boldsymbol{u};\Lambda,\Phi) &= (\varepsilon_k\nabla k,\nabla\varphi_k)_\Omega + \left(\frac{3k}{2\Delta t} + (\overline{\boldsymbol{w}}\cdot\nabla)k + 2\beta^*\widehat{\omega}^n k,\varphi_k\right)_\Omega\\
&\quad + (\varepsilon_\omega\nabla\omega,\nabla\varphi_\omega)_\Omega + \left(\frac{3\omega}{2\Delta t} + (\overline{\boldsymbol{w}}\cdot\nabla)k + 2\beta\widehat{\omega}^n\omega,\varphi_\omega\right)_\Omega,
\end{aligned} \tag{4.51}$$

$$\begin{aligned}
L^{k\omega}(\Phi) &= \Big(\frac{4\widehat{k}^n - \widehat{k}^{n-1}}{2\Delta t} + \widehat{P_k(t_n)} + \beta^*\widehat{k}^n\widehat{\omega}^n,\varphi_k\Big)_\Omega\\
&\quad + \Big(\frac{4\widehat{\omega}^n - \widehat{\omega}^{n-1}}{2\Delta t} + \beta(\widehat{\omega}^n)^2 + \widehat{P_\omega(t_n)} + \widehat{C_D(t_n)},\varphi_\omega\Big)_{\Omega_\Delta}.
\end{aligned} \tag{4.52}$$

Because of the SUPG and DC stabilization, we define the forms

$$\begin{aligned}
B^{k\omega}_{SUPG}(\boldsymbol{u};\Lambda,\Phi) &= \sum_{K\in\mathcal{T}_\Delta}\delta_{Kk}\Big(\frac{3k}{2\Delta t} + \overline{\boldsymbol{w}}\cdot\nabla k + 2\beta^*\widehat{\omega}^n k + \nabla\cdot(\varepsilon_k\nabla k),\overline{\boldsymbol{w}}\cdot\nabla\varphi_k\Big)_K\\
&\quad + \sum_{K\in\mathcal{T}_\Delta}\delta_{K\omega}\Big(\frac{3\omega}{2\Delta t} + \overline{\boldsymbol{w}}\cdot\nabla\omega + 2\beta\widehat{\omega}^n\omega + \nabla\cdot(\varepsilon_\omega\nabla\omega),\overline{\boldsymbol{w}}\cdot\nabla\varphi_\omega\Big)_K,
\end{aligned} \tag{4.53}$$

$$\begin{aligned}
L^{k\omega}_{SUPG}(\boldsymbol{u};\Phi) &= \sum_{K\in\mathcal{T}_\Delta}\delta_{Kk}\Big(\frac{4\widehat{k}^n - \widehat{k}^{n-1}}{2\Delta t} + \widehat{P_k(t_n)} + \beta^*\widehat{k}^n\widehat{\omega}^n,\overline{\boldsymbol{w}}\cdot\nabla\varphi_k\Big)_K\\
&\quad + \sum_{K\in\mathcal{T}_\Delta}\delta_{K\omega}\Big(\frac{4\widehat{\omega}^n - \widehat{\omega}^{n-1}}{2\Delta t} + \beta(\widehat{\omega}^n)^2 + \widehat{P_\omega(t_n)} + \widehat{C_D(t_n)},\overline{\boldsymbol{w}}\cdot\nabla\varphi_k)\Big)_K,
\end{aligned} \tag{4.54}$$

$$B_{DC}^{k\omega}(\boldsymbol{u};\Lambda^*,\Phi)=\sum_{K\in\mathcal{T}_\Delta}\Big(\alpha_{Kk}\nabla k,\nabla\varphi_k\Big)_K+\sum_{K\in\mathcal{T}_\Delta}\Big(\alpha_{K\omega}\nabla\omega,\nabla\varphi_\omega\Big)_K$$
$$+\sum_{K\in\mathcal{T}_\Delta}\int_K\left((\alpha_{Kk}-\alpha'_{Kk})^+-\alpha_{Kk}\right)\nabla k\cdot\left(\frac{\overline{\boldsymbol{w}}\otimes\overline{\boldsymbol{w}}}{\|\overline{\boldsymbol{w}}\|_K^2}\right)\nabla\varphi_k dx$$
$$+\sum_{K\in\mathcal{T}_\Delta}\int_K\left((\alpha_{K\omega}-\alpha'_{K\omega})^+-\alpha_{K\omega}\right)\nabla\omega\cdot\left(\frac{\overline{\boldsymbol{w}}\otimes\overline{\boldsymbol{w}}}{\|\overline{\boldsymbol{w}}\|_K^2}\right)\nabla\varphi_\omega dx. \tag{4.55}$$

We use the following notation. The parameters δ_{Kk},$\delta_{K\omega}$ are defined by

$$\delta_{Kk}=\left(\frac{4\|\varepsilon_k\|_K}{h_K^2}+\frac{2\|\overline{\boldsymbol{w}}\|_K}{h_K}+2\beta^*\|\widehat{\omega}^n\|_K\right)^{-1},$$
$$\delta_{K\omega}=\left(\frac{4\|\varepsilon_\omega\|_K}{h_K^2}+\frac{2\|\overline{\boldsymbol{w}}\|_K}{h_K}+2\beta\|\widehat{\omega}^n\|_K\right)^{-1}. \tag{4.56}$$

The discontinuity capturing coefficients $\alpha'_{Kk\omega}$ and $\alpha'_{K\omega}$ are determined by

$$\alpha'_{Kk}=\delta_{Kk}\ \|\overline{\boldsymbol{w}}\|_K,\qquad \alpha'_{K\omega}=\delta_{K\omega}\|\overline{\boldsymbol{w}}\|_K. \tag{4.57}$$

The definitions of the discontinuity capturing coefficients α_{Kk} and $\alpha_{K\omega}$ are based on the local element residuals

$$\mathrm{res}_1(k^*)=\frac{3k^*-4\widehat{k}^n+\widehat{k}^{n-1}}{2\Delta t}+\overline{\boldsymbol{w}}\cdot\nabla k^*+2\beta^*\widehat{\omega}^n k^*-\beta^*\widehat{\omega}^n\widehat{k}^n-\widehat{P_k(t_n)}-\nabla\cdot(\varepsilon_k\nabla k^*) \tag{4.58}$$

and

$$\mathrm{res}_2(\omega^*)=\frac{3\omega^*-4\widehat{\omega}^n+\widehat{\omega}^{n-1}}{2\Delta t}+\overline{\boldsymbol{w}}\cdot\nabla\omega^*+2\beta\widehat{\omega}^n\omega^*-\beta^*(\widehat{\omega}^n)^2-\widehat{P_\omega(t_n)}-\widehat{C_D(t_n)}$$
$$-\nabla\cdot(\varepsilon_\omega\nabla\omega^*). \tag{4.59}$$

We set

$$\alpha_{Kk}=\alpha_{Kk}(k^*)=\frac{1}{2}A_{Kk}(k^*)h_K\frac{\|\mathrm{res}_1(k^*)\|_K}{\|\nabla k^*\|_K}, \tag{4.60}$$
$$\alpha_{K\omega}=\alpha_{K\omega}(\omega^*)=\frac{1}{2}A_{K\omega}h_K(\omega^*)\frac{\|\mathrm{res}_2(\omega^*)\|_K}{\|\nabla\omega^*\|_K}, \tag{4.61}$$

if $\|\nabla k^*\|_K\neq 0$ and $\|\nabla\omega^*\|_K\neq 0$, otherwise,

$$\alpha_{Kk=0},\qquad \alpha_{K\omega}=0. \tag{4.62}$$

Here,

$$A_{Kk}(k^*)=\left(0.7-\frac{2\varepsilon_k}{\|\mathbf{a}_1\|_K h_K}\right)^+,\qquad A_{K\omega}=\left(0.7-\frac{2\varepsilon_\omega}{\|\mathbf{a}_2\|_K h_K}\right)^+, \tag{4.63}$$

with

$$\mathbf{a}_1 = \frac{\mathrm{res}_1(k^*)}{\|\nabla k^*\|_K^2}\nabla k^*, \qquad \mathbf{a}_2 = \frac{\mathrm{res}_2(\omega^*)}{\|\nabla \omega^*\|_K^2}\nabla^* \omega. \tag{4.64}$$

Finally, we define the stabilized $k-\omega$ turbulence model forms $B_{TM} = B_{TM}^{k\omega}$ and $L_{TM} = L_{TM}^{k\omega}$:

$$B_{TM}^{k\omega}(\boldsymbol{u};\Lambda^*,\Lambda,\Phi) = B_{k\omega}(\boldsymbol{u};\Lambda,\Phi) + B_{SUPG}^{k\omega}(\boldsymbol{u};\Lambda,\Phi) + B_{DC}^{k\omega}(\boldsymbol{u};\Lambda^*,\Lambda,\Phi), \tag{4.65}$$

$$L_{TM}^{k\omega}(\boldsymbol{u};\Phi) = L_{k\omega}(\Phi) + L_{SUPG}^{k\omega}(\boldsymbol{u};\Phi). \tag{4.66}$$

4.4.1 The solution of the problem for computing the quantities k and ω

Now we shall introduce the discrete problem for the determination of the approximations to the functions k and ω at time t_{n+1}, provided the approximate solution has already been computed on previous time levels. We use again the finite-dimensional spaces $\mathcal{V}_\Delta$ and $\mathcal{V}_\Delta^0$ defined by (4.20) and set $\mathcal{V}_\Delta^\omega = \mathcal{V}_\Delta^k = \mathcal{V}_\Delta^0$.

The nonlinear stabilization problem reads: Find $\Lambda_\Delta = (k_\Delta, \omega_\Delta) \in [\mathcal{V}_\Delta]^2$ satisfying conditions (2.19) a), b) at the vertices lying on $\Gamma_{D\Delta} \cup \Gamma_{W\Delta}$ and

$$B_{TM}^{k\omega}(\boldsymbol{u};\Lambda_\Delta,\Lambda_\Delta,\Phi_\Delta) = L_{TM}^{k\omega}(\boldsymbol{u};\Phi_\Delta), \quad \forall \Phi_\Delta = (\varphi_{k\Delta}, \varphi_{\omega\Delta}) \in \mathcal{V}_\Delta^k \times \mathcal{V}_\Delta^\omega. \tag{4.67}$$

4.4.2 The solution of the complete discrete $k-\omega$ turbulent flow problem at time t_{n+1}

We want to find $U_\Delta = (\boldsymbol{u}_\Delta, p_\Delta)$, $\Lambda_\Delta = (k_\Delta, \omega_\Delta)$ and $\nu_{T\Delta}$ such that the following conditions are satisfied:

a) U_Δ satisfies (4.40), a).
b) $\Lambda_\Delta = (k_\Delta, \omega_\Delta) \in [\mathcal{V}_\Delta]^2$ satisfies conditions (2.19), a) at the vertices lying on $\Gamma_{D\Delta} \cup \Gamma_{W\Delta}$ and (4.67).
c) The relation $\nu_{T\Delta} = k_\Delta / \omega_\Delta$ is satisfied.

4.4.3 Algorithm for the solution of the discrete $k-\omega$ turbulent flow problem at time t_{n+1}

(0) In the beginning of the time marching process set $n = 0$, $U_\Delta^{-1} = U_\Delta^0 = (\boldsymbol{u}^0, p_{ref})$, $\nu_{T\Delta}^{-1} = \nu_{T\Delta}^0 = \nu$, $k_\Delta^{-1} = k_\Delta^0 = 10\nu$, $\omega_\Delta^{-1} = \omega_\Delta^0 = 10$ (see the conditions specified in (2.7) and Section 2.5). Then find $\Lambda_\Delta^* = (k_\Delta^*, \omega_\Delta^*) \in [\mathcal{V}_\Delta]^2$ satisfying conditions (2.19), a), b) at vertices lying on $\Gamma_{D\Delta} \cup \Gamma_{W\Delta}$ and

$$B^{k\omega}(\boldsymbol{u}_\Delta^0;\Lambda_\Delta^*,\Phi_\Delta) + B_{SUPG}^{k\omega}(\boldsymbol{u}_\Delta^0;\Lambda_\Delta^*,\Phi_\Delta) = L_{TM}^{k\omega}(\boldsymbol{u}_\Delta^0,\Phi_\Delta) \quad \forall \Phi_\Delta \in \mathcal{V}_\Delta^k \times \mathcal{V}_\Delta^\omega. \tag{4.68}$$

(1) Let $\varepsilon > 0$ be given. Let the approximation Ω_Δ of the domain $\Omega_{t_{n+1}}$ and $\boldsymbol{w}_\Delta^{n+1}$, $\widehat{\boldsymbol{u}}_\Delta^{n-1}$, $\widehat{\boldsymbol{u}}_\Delta^n$, $\widehat{k}_\Delta^{n-1}$, $\widehat{k}_\Delta^n$, $\widehat{\omega}_\Delta^{n-1}$, $\widehat{\omega}_\Delta^n$, $\widehat{\nu}_{T\Delta}^n$, $\widehat{P_k(t_n)}$, $\widehat{P_\omega(t_n)}$, $\widehat{C_D(t_n)}$ (quantities transformed to the domain Ω_Δ by Remark 4.1) have already been determined. Set $U_\Delta^* = (\widehat{\boldsymbol{u}}_\Delta^n, \widehat{p}_\Delta^n)$, $k_\Delta^* := \widehat{k}_\Delta^n$, $\omega_\Delta^* := \widehat{\omega}_\Delta^n$, $\nu_{T\Delta}^* := \widehat{\nu}_{T\Delta}^n = k_\Delta^* / \omega_\Delta^*$.

(2) Find $U_\Delta = (\boldsymbol{u}_\Delta, p_\Delta) \in W_\Delta \times Q_\Delta$ such that $\boldsymbol{u}$ satisfies the boundary conditions (2.6) at nodes on $\Gamma_{D\Delta} \cup \Gamma_{W\Delta}$ and

$$\begin{aligned} &a_{NS}(\nu_{T\Delta}^*, U_\Delta^*, U_\Delta, V_\Delta) + \ell_{NS}(\nu_{T\Delta}^*, U_\Delta^*, U_\Delta, V_\Delta) + P_{NS}(U_\Delta, V_\Delta) \\ &= f_{NS}(V_\Delta) + F_{NS}(V_\Delta) \qquad \forall V_\Delta \in X_\Delta \times Q_\Delta. \end{aligned} \tag{4.69}$$

(3) Find $\Lambda_\Delta = (k_\Delta, \omega_\Delta) \in [\mathcal{V}_\Delta]^2$ satisfying conditions (2.19, a), b) at vertices lying on $\Gamma_{D\Delta} \cup \Gamma_{W\Delta}$ and

$$B_{TM}^{k\omega}(\boldsymbol{u}_\Delta, \Lambda_\Delta^*, \Lambda_\Delta, \Phi_\Delta) = L_{TM}^{k\omega}(\boldsymbol{u}_\Delta, \Phi_\Delta) \quad \forall \Phi_\Delta = (\varphi_{k\Delta}, \varphi_{\omega\Delta}) \in \mathcal{V}_\Delta^k \times \mathcal{V}_\Delta^\omega. \tag{4.70}$$

(4) Set $\nu_{T\Delta} := k_\Delta / \omega_\Delta$.

(5) If

$$\|\nu_{T\Delta}^* - \nu_{T\Delta}\| < \varepsilon \quad \text{and} \quad \|U_\Delta^* - U_\Delta\| < \varepsilon, \tag{4.71}$$

then set

$$U_\Delta^{n+1} := U_\Delta, \qquad k_\Delta^{n+1} := k_\Delta, \qquad \omega_\Delta^{n+1} := \omega_\Delta, \qquad \nu_{T\Delta}^{n+1} := k_\Delta / \omega_\Delta, \tag{4.72}$$

else

$$U_\Delta^* := U_\Delta, \qquad k_\Delta^* := k_\Delta, \qquad \omega_\Delta^* := \omega_\Delta, \qquad \nu_{T\Delta}^* k_\Delta^* / \omega_\Delta^*, \tag{4.73}$$

and go to (2).

5 The realization of the coupled fluid-structure interaction problem

In this section we shall describe the algorithm of the numerical realization of the complete fluid-structure interaction problem.

5.1 Construction of the ALE mapping for three degrees of freedom

The ALE mapping is constructed with the use of the linear equations describing the deformation of elastic bodies:

$$\nabla[(\lambda + \mu)\nabla \cdot \boldsymbol{d}] + \nabla \cdot (\mu \nabla \boldsymbol{d}) = 0 \quad \text{in } \Omega_0, \tag{5.1}$$

where $\boldsymbol{d} = (d_1, d_2)$ is a displacement defined in Ω_0. The Lamé coefficients λ and μ are computed by

$$\lambda = \frac{E_a \sigma_a}{(1+\sigma_a)(1-2E_a)}, \qquad \mu = \frac{E_a}{2+2\sigma_a}, \tag{5.2}$$

where E_a is an artificial Young modulus and σ_a is an artificial Poisson ratio.

The boundary conditions for $\boldsymbol{d}$ are prescribed by

$$\boldsymbol{d}|_{\Gamma_D\cup\Gamma_O}=0 \tag{5.3}$$

and on Γ_{W_0} they are determined by the functions $h(t)$, $\alpha(t)$, $\beta(t)$:

$$\begin{aligned} d_1&=X_1\cos\alpha-X_2\sin\alpha,\\ d_2&=X_1\sin\alpha+X_2\cos\alpha+h, \end{aligned}\qquad Y=(X_1,X_2)\in P_0, \tag{5.4}$$

for the main part of the airfoil and

$$\begin{aligned} d_1&=X_1\cos(\alpha+\beta)-X_2\sin(\alpha+\beta)+d_{PF}\cos\alpha,\\ d_2&=X_1\sin(\alpha+\beta)+X_2\cos(\alpha+\beta)+d_{PF}\sin\alpha+h, \end{aligned}\qquad Y=(X_1,X_2)\in F_0, \tag{5.5}$$

for the flap of the airfoil.

The solution of equations (5.1) gives us the ALE mapping of $\overline{\Omega}_0$ onto $\overline{\Omega}_t$ by the relation

$$\mathcal{A}_t(Y)=Y+\boldsymbol{d}(Y),\qquad Y\in\overline{\Omega}_0, \tag{5.6}$$

for each time t.

System (5.1) is discretized by the conforming piecewise linear finite elements on the mesh $\mathcal{T}_\Delta^0$ used for computing the velocity and pressure fields in the beginning of the computational process in the polygonal approximation $\Omega_{0\Delta}$ of the domain Ω_0.

We introduce the finite element spaces

$$\begin{aligned} \mathcal{X}_\Delta&=\{\boldsymbol{d}_\Delta=(d_{\Delta1},d_{\Delta2});d_{\Delta i}|_K\in P^1(K)\ \forall K\in\mathcal{T}_\Delta^0,\ i=1,2\},\\ \mathcal{V}_\Delta&=\{\boldsymbol{\varphi}_\Delta\in\mathcal{X}_\Delta;\boldsymbol{\varphi}_\Delta(Y)=0 \text{ for all vertices } Y\in\partial\Omega_0\}, \end{aligned} \tag{5.7}$$

and the form

$$B_\Delta(\boldsymbol{d}_\Delta,\boldsymbol{\varphi}_\Delta)=((\lambda+\mu)(\nabla\cdot\boldsymbol{d}_\Delta),(\nabla\cdot\boldsymbol{\varphi}_\Delta))_{\Omega_{0\Delta}}+(\mu\nabla\boldsymbol{d},\nabla\boldsymbol{\varphi}_\Delta)_{\Omega_{0\Delta}}. \tag{5.8}$$

Then the approximate solution of problem (5.1), (5.3)-(5.5) is defined as a function $\boldsymbol{d}_\Delta\in\mathcal{X}_\Delta$ satisfying the Dirichlet boundary conditions defined by (5.3)-(5.5) with the values of h, α, β at time t_{n+1} and considered at the vertices lying on $\partial\Omega_0$ and the identity

$$B_\Delta(\boldsymbol{d}_\Delta,\boldsymbol{\varphi}_\Delta)=0\qquad\forall\boldsymbol{\varphi}_\Delta\in\mathcal{V}_\Delta. \tag{5.9}$$

It is possible to choose the Lamé coefficients λ and μ as constants, but it is more suitable to define them by (5.2), where the parameters E_a and σ_a are piecewise constant on the mesh $\mathcal{T}_\Delta^0$. We define them by

$$\sigma_a|_K=0.25,\qquad E_a|_K=\frac{1}{\text{meas}(K)}, \tag{5.10}$$

where meas(K) denotes the area of an element K. The mesh around the airfoil is typically refined into smaller triangles. Since smaller triangles imply the larger Young modulus E_a in (5.10), the mesh around the airfoil moves with the airfoil and its deformation is small.

If the displacement $\boldsymbol{d}_\Delta$ is computed at time t_{n+1}, then, in view of (5.6), the approximation of the ALE mapping is obtained in the form

$$\mathcal{A}_{t_{n+1}\Delta}(Y) = Y + \boldsymbol{d}_\Delta(Y), \qquad Y \in \Omega_{0\Delta}. \tag{5.11}$$

Of course, in practical computations, this formula is applied to vertices Y of the triangulation $\mathcal{T}_\Delta^0$ only and $\mathcal{A}_{t_{n+1}\Delta}$ is defined as a piecewise linear mapping.

The knowledge of the ALE mapping at the time instants t_{n-1}, t_n, t_{n+1} allows us to approximate the domain velocity with the aid of the second-order backward difference formula

$$\boldsymbol{w}_\Delta^{n+1}(x) = \frac{3x - 4\mathcal{A}_{t_n\Delta}(\mathcal{A}^{-1}_{t_{n+1}\Delta}(x)) + \mathcal{A}_{t_{n-1}\Delta}(\mathcal{A}^{-1}_{t_{n+1}\Delta}(x))}{2\tau}, \quad x \in \Omega_{t_{n+1}\Delta}. \tag{5.12}$$

5.2 Discretization of the structural problem

In order to solve equations (3.1) of motion describing the airfoil vibrations, we transform them to a first-order system. We introduce the following notation:

$$\boldsymbol{Z}(t) = (\dot{h}(t), \dot{\alpha}(t), \dot{\beta}(t))^T, \qquad \boldsymbol{f} = (\mathcal{L}, \mathcal{M}_\alpha, \mathcal{M}_\beta)^T, \tag{5.13}$$

$$\mathbb{K} = \begin{pmatrix} k_{hh} & 0 & 0 \\ 0 & k_{\alpha\alpha} & 0 \\ 0 & 0 & k_{\beta\beta} \end{pmatrix}, \qquad \mathbb{D} = \begin{pmatrix} D_{hh} & 0 & 0 \\ 0 & D_{\alpha\alpha} & 0 \\ 0 & 0 & D_{\beta\beta} \end{pmatrix}, \tag{5.14}$$

$$\mathbb{M} = (M_{ij})_{i,j=1}^3, \tag{5.15}$$

where the components of the nonlinear mass matrix $\mathbb{M} = \mathbb{M}(\boldsymbol{Z})$ read

$$\begin{aligned} &M_{11} = m, && M_{12} = (S_\alpha - S_\beta)\cos\alpha + S_\beta\cos(\alpha+\beta), && M_{13} = S_\beta\cos(\alpha+\beta), \\ &M_{21} = M_{12}, && M_{22} = I_\alpha - 2d_{PF}S_\beta + 2d_{PF}S_\beta\cos\beta, && M_{23} = I_\beta + d_{PF}S_\beta\cos\beta, \\ &M_{31} = M_{13}, && M_{32} = M_{23}, && M_{33} = I_\beta. \end{aligned} \tag{5.16}$$

Further, we introduce the following notation: $\mathbb{O}$ – zero 3×3 matrix, $\mathbb{I}$ – unit 3×3 matrix, $\boldsymbol{0}$ – 3-dimensional zero vector and $\boldsymbol{g}$ – the vector of nonlinearities:

$$\boldsymbol{g} = \begin{pmatrix} (S_\alpha - S_\beta)\dot{\alpha}^2\sin\alpha + S_\beta(\dot{\alpha}+\dot{\beta})^2\sin(\alpha+\beta) \\ d_{PF}S_\beta\dot{\beta}^2\sin\beta + 2(d_{PF}S_\beta)\dot{\alpha}\dot{\beta}\sin\beta \\ -d_{PF}S_\beta\dot{\alpha}^2\sin\beta \end{pmatrix}. \tag{5.17}$$

Then system (3.1) is equivalent to the first-order system

$$\dot{\boldsymbol{Z}} = \boldsymbol{h}(t, \boldsymbol{Z}), \tag{5.18}$$

where $\boldsymbol{h}$ is the vector function defined by

$$\boldsymbol{h}(t,\boldsymbol{Z})=\begin{pmatrix}\mathbb{M}^{-1}(\boldsymbol{Z}) & \mathbb{O}\\ \mathbb{O} & \mathbb{I}\end{pmatrix}\left(\begin{pmatrix}\boldsymbol{f}(t)\\ \boldsymbol{0}\end{pmatrix}-\begin{pmatrix}\mathbb{D} & \mathbb{O}\\ \mathbb{O} & \mathbb{K}\end{pmatrix}\boldsymbol{Z}+\begin{pmatrix}\boldsymbol{g}\\ \boldsymbol{0}\end{pmatrix}\right). \tag{5.19}$$

This system is equipped with the initial condition prescribing the value $\boldsymbol{Z}(0)$ given by conditions (3.2). The initial value problem for system (5.18) is solved by the fourth-order Runge-Kutta method. In the step from t_n to t_{n+1} one needs the evaluation of the values $\boldsymbol{f}(\hat{t})$ at discrete instants $\hat{t}\in[t_n,t_{n+1}]$. They are obtained by a linear extrapolation from the interval $[t_{n-1},t_n]$ to $[t_n,t_{n+1}]$. If the values $\boldsymbol{f}(t_n)$ and $\boldsymbol{f}(t_{n+1})$ have already been approximated, then $\boldsymbol{f}(\hat{t})$ is computed by the linear interpolation in the interval $[t_n,t_{n+1}]$.

5.3 Computation of aerodynamic forces acting on the airfoil

In the case when the flap is not separated from the main body of the airfoil, the aerodynamic forces $\mathcal{L}$, $\mathcal{M}_\alpha$, $\mathcal{M}_\beta$ at time t_{n+1} are computed from (3.3)-(3.5) by using the approximation of the stress tensor (3.6) known from the solution $U_\Delta=(\boldsymbol{u}_\Delta,p_\Delta)$ of the stabilized discrete flow problem (4.40) and extrapolated to the boundary. The integrals in (3.3)-(3.5) are computed with the aid of numerical quadratures. In the case, when the flap is separated from the main body of the airfoil, i.e. $P_t\cap F_t=\emptyset$, the force and moments can be computed on the basis of a weak formulation similarly as in Sváček et al. [47].

5.4 Coupling procedure

In the solution of the complete coupled fluid-structure interaction problem it is necessary to apply a suitable coupling procedure. See, e.g. Badia and Codina [1] for a general framework. Here we apply the following algorithm.

(0) Prescribe $\varepsilon>0$ – the measure of accuracy in the coupling procedure, and an integer $M\geq 0$ – the maximal number of iterations in the coupling procedure.
(1) Assume that the solution $U_\Delta=(\boldsymbol{u}_\Delta,p_\Delta)$ of the discrete flow problem (4.40) and the force $\mathcal{L}$ and torsional moments $\mathcal{M}_\alpha$ and $\mathcal{M}_\beta$ computed from (3.3)-(3.5) are known at time levels t_{n-1} and t_n.
(2) Extrapolate linearly $\mathcal{L}$, $\mathcal{M}_\alpha$ and $\mathcal{M}_\beta$ from the interval $[t_{n-1},t_n]$ to $[t_n,t_{n+1}]$. Set $m:=0$.
(3) *Prediction of* h,α,β: Compute the displacement h and the angles α and β at time t_{n+1} as the solution of system (5.18) by the Runge-Kutta method. Denote it by h^*, α^*, β^*.
(4) On the basis of h^*,α^*,β^* determine the position of the airfoil at time t_{n+1}, the domain $\Omega_{t_{n+1}\Delta}$, the ALE mapping $\mathcal{A}_{t_{n+1}\Delta}$ and the domain velocity $\boldsymbol{w}_\Delta^{n+1}$.
(5) Solve the nonlinear discrete stabilized problem (4.40) at time t_{n+1} by the Oseen-like iterative algorithm 4.3.2.
(6) *Correction of* h, α, β: Compute $\mathcal{L}$, $\mathcal{M}_\alpha$ and $\mathcal{M}_\beta$ from (3.3)-(3.5) at time t_{n+1} and interpolate $\mathcal{L}$, $\mathcal{M}_\alpha$ and $\mathcal{M}_\beta$ on $[t_n,t_{n+1}]$. Compute h, α, β at time t_{n+1} from (5.18) by the Runge-Kutta method.

(7) If $|h^*-h|+|\alpha^*-\alpha|+|\beta^*-\beta|\geq\varepsilon$ and $m<M$, set $h^*=h$, $\alpha^*=\alpha$, $\beta^*=\beta$, $m:=m+1$ and go to 4. Otherwise, $n:=n+1$ and go to (2).

If $M=0$, then we get a loose (weak) coupling of the flow and structural problems. With increasing M and decreasing ε, the coupling becomes stronger.

Remark 5.1. The assumption that the approximate solution U_Δ and the quantities $\mathcal{L}$, $\mathcal{M}_\alpha$, $\mathcal{M}_\beta$ are known at time instants t_{n-1} and t_n is satisfied in practical computations, because the computational process starts with a fixed airfoil and flap, which are released after several time steps.

Remark 5.2. It follows from the above algorithm that on different time levels different meshes are used. However, in our case it is not necessary to use a complete remeshing, because the mesh is only deformed, as follows from Section 5.1. The complete remeshing is necessary in the case, when the mesh becomes strongly distorted, which happens only rarely, when the vibration amplitudes become very large. In this situation, some mesh patterns can be constructed in advance before the FSI process and used only if needed.

On the other hand, there is a question, if it is suitable to apply techniques that do not require mesh updating in time, as, for example, the fictitious domain method (see, e.g., [22]), because the meshes have to be strongly refined around the moving airfoil (see Fig. 2), in order to get an accurate resolution of aerodynamical forces acting on the airfoil.

6 Numerical experiments

We performed computations for the airfoil configurations considered in [28], where the authors computed the stability bounds of a wing profile model by MSC.NASTRAN, which is based on a linear description of the structure behaviour.

The numerical simulation was carried out for the airfoil NACA 0012 of the total length (including the gap and flap – see Fig. 1) $c=0.3$ m. The axes EA and EF are placed at 40% and 80%, respectively, of the length of the whole airfoil measured from the leading edge. The following structural parameters in equations (3.1) were used:

$$\begin{aligned}
&m=0.086622\text{kg}, && k_{hh}=105.109\text{N/m},\\
&k_{\alpha\alpha}=3.69558\text{Nm/rad}, && k_{\beta\beta}=0.2\text{Nm/rad},\\
&S_\alpha=-0.000779598\text{kgm}, && S_\beta=0\text{kgm},\\
&I_\alpha=0.000487291\text{kgm}^2, && I_\beta=0.0000341104\text{kgm}^2,\\
&d_{PF}=0.140001\text{m}, && l=0.079\text{m}.
\end{aligned}$$

The damping coefficients D_{hh}, $D_{\alpha\alpha}$, $D_{\beta\beta}$ were assumed to be zero. The gap between the main lifting surface and the flap was varied from $g=0\%$ to $g=7\%$ of the flap chord length $L_f=0.068$ m.

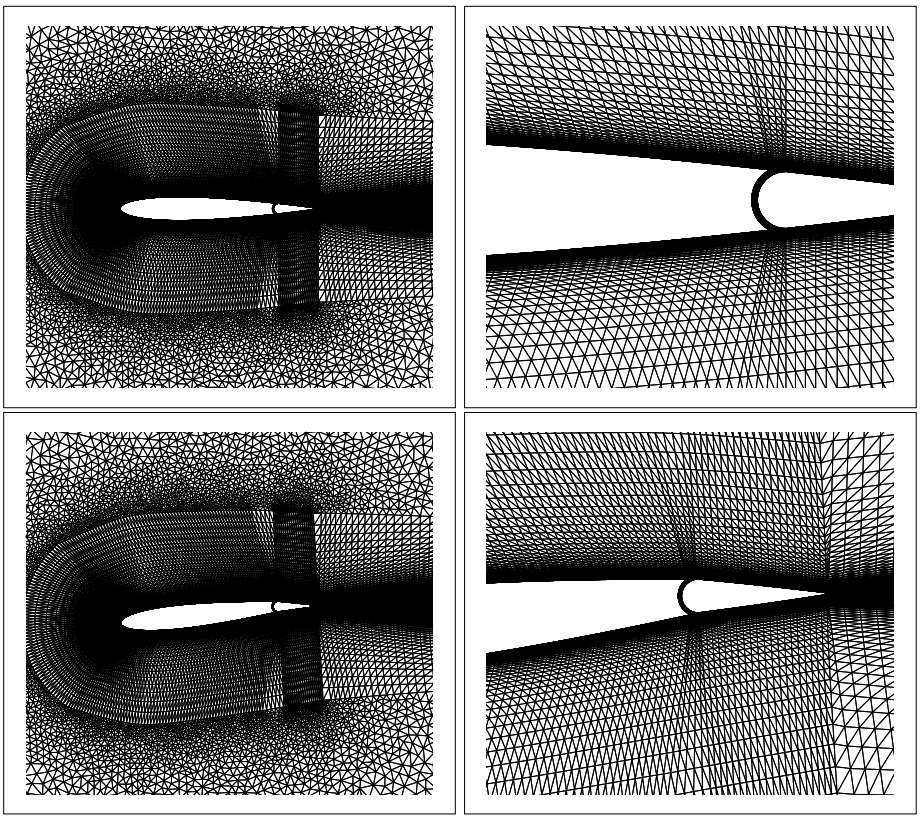

Figure 2: Detail of anisotropically adapted mesh for NACA 0012 airfoil for the gap $g=2.4\%$ (nondeformed and deformed position).

Fig. 2 shows examples of the triangulation around the airfoil in the channel. The mesh was anisotropically adapted by the method described in [9], using the combination of the software Angener [8] and the open source software GMSH [18, 19]. The total number of fluid finite elements was approximately 60 000 depending on the gap size.

The structural initial conditions in all computations were set to

$$h(0)=-1.5 \text{ mm}, \alpha(0)=1^\circ \text{ for } g\le 1.26\% \quad \text{or} \quad h(0)=-5 \text{ mm}, \alpha(0)=3^\circ \text{ for } g>1.26\%$$
$$\text{and} \quad \beta(0)=\dot{h}(0)=\dot{\alpha}(0)=\dot{\beta}(0)=0. \tag{6.1}$$

The computational process started from the solution of the flow past a fixed airfoil at time $t=-0.01$ s. At time $t=0$ the airfoil was released and the computation of the real interaction started. (Cf. Remark 5.1.) Computations were carried out with the time step $\tau=0.01c/U_\infty$ for the kinematic viscosity $\nu=1.5\cdot10^{-5}$ m^2/s, the air density $\rho=1.225$ kg/m^3 and the far-field flow velocity $U_\infty=6-12$ m/s corresponding to the Reynolds numbers between $1.2\cdot10^5$ and $2.4\cdot10^5$. The computational process was finished either by approaching time $T=2$ s in aeroelastic stable cases or if the process failed due to high vibration amplitudes, when the aeroelastic instability appeared for the unstable limit cycle oscillation

(LCO) and the amplitude of the flap exceeded a limit value by which the computational mesh was degenerated. The total computer time for the computation of the responses $h(t)$, $\alpha(t)$, $\beta(t)$ for $t=0-2$ s on a PC with Intel i7 processor and 4GB memory was about 3 days.

This shows that the developed method is applicable to a complicated FSI problem even on a PC, but at the cost of a long CPU time. The most demanding part of the computational process is formed by the realization of linearized problems. Of course, for practical applications it is necessary to apply the method on high-performance computers. It is also suitable to use parallel processes, e.g., in the solution of the construction of linear systems and their solution. However, this is out of the subject of this paper.

The frequency analysis of the dynamic response was carried out with the aid of the Fourier transform

$$G(f_n)=\int_0^T g(t)e^{-2\pi i f_n t}\,\mathrm{d}t \tag{6.2}$$

with $g=h$, α or β, and $f_n=n\Delta f\in[0,50]$, $\Delta f=0.1$ Hz, approximated by the rectangle formula

$$G(f_n)=\sum_{k=0}^{N-1} g(t_k)e^{-2\pi i f_n t_k}\Delta t. \tag{6.3}$$

Here i is the imaginary unit, $\Delta t=T/N$ and N is the number of time steps in the interval $[0,T)$. The results of the frequency analysis are shown in graphs of the quantity

$$|G(f_n)|=\sqrt{\Re^2(G(f_n))+\Im^2(G(f_n))}.$$

6.1 Numerical results – flutter analysis

Figs. 3-7 show examples of the computed functions $h(t)$, $\alpha(t)$, $\beta(t)$, the corresponding spectra and the phase diagrams for Spalart-Allmaras and $k-\omega$ turbulence models and several far-field flow velocities U_∞. For the smaller flow velocity the amplitudes for the vertical displacement h and the rotations α, β are decreasing in time and the system is stable (see Fig. 3). The spectra show three frequencies that belong to the vertical motion of the airfoil and to the rotations the main lifting part of the profile and of the flap. The lowest frequency at about 5.5 Hz belongs to the vertical airfoil motion h and the two higher frequencies at about 12 Hz and 15 Hz belong to the airfoil and the flap rotations α and β, respectively. Comparing the results in Figs. 3-5 we can see that the damping of vibrations decreases with the far-field flow velocity and is lower for the Spalart-Allmaras turbulence model than for the $k-\omega$ model. Nevertheless, the system is still stable in all three cases presented in these figures. By increasing the far-field flow velocity up to $U_\infty=11$ m/s the vibration regime can be considered as LCO with a small amplitude less than 3 degrees for the flap rotation β and the highest frequency belonging to this motion becomes the most dominant in the spectra (see Fig. 6). The system is still stable, if the model $k-\omega$ is used, but a "catastrophic" type of flutter with a negative damping

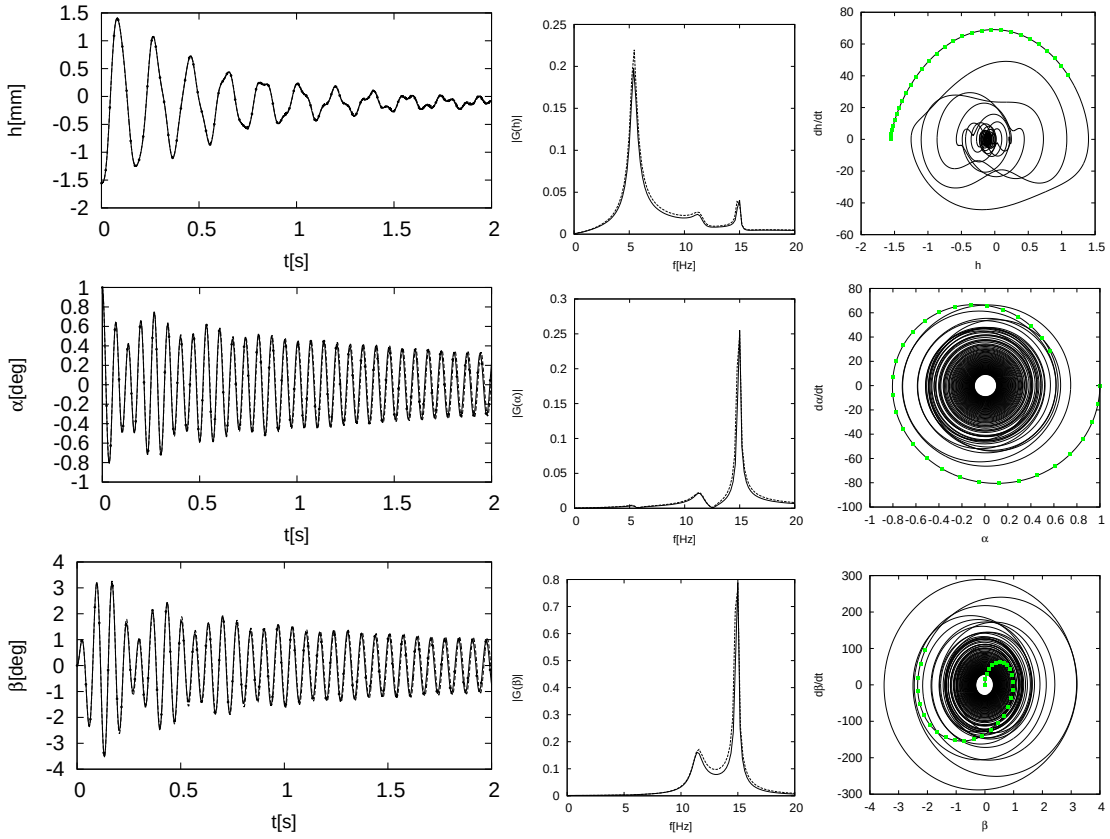

Figure 3: Airfoil with gap 0.54%: Functions $h(t)$, $\alpha(t)$, $\beta(t)$ (left), their spectra (middle) and phase diagrams (right) for $k-\omega$ turbulence model and far-field airflow velocity 7 m/s.

and quickly increasing vibration amplitudes appear in this case according to the Spalart-Allmaras turbulence model. For the higher flow velocity $U_\infty = 12$ m/s, the system is becoming unstable by a "catastrophic" flutter also by using the $k-\omega$ model (see Fig. 7). In this case, the rotation amplitudes are increasing very fast and the angle β for the flap reaches values up to about 5 degrees after about 2 s oscillating with the dominant flutter frequency of about 15 Hz.

These results are in agreement with the NASTRAN computations, according to which the system becomes unstable by flutter in torsion for the far-field flow velocity at 11.3 m/s and the flutter frequency $f_{cr} = 14.9$ Hz (see Table 1 and [28, 29]).

The functions $h(t)$, $\alpha(t)$, $\beta(t)$ computed by the Spalart-Allmaras turbulence model and the $k-\omega$ turbulence model are compared in Fig. 8. Both models give nearly identical results in the beginning of the transient regime just after releasing the airfoil at the time $t = 0$ s. However, after about 1 s the differences in the vibration amplitudes for the two turbulence models are getting remarkable. The $k-\omega$ turbulence model gives smaller vibration amplitudes. The airfoil is more damped by the aerodynamic forces computed

Table 1: Comparison of the results computed by NASTRAN without considering the gap between the airfoil and the flap [28, 29] and by the developed finite element method for eigen-frequencies f (computed by the FEM for the gap 0.54%), for far-field airflow velocity 6 m/s, for critical flutter velocities U_F and flutter frequencies f_{cr}.

	h – bending f [Hz]	β – flap torsion f [Hz]	α – torsion f [Hz]	U_F [m/s]	f_{cr} [Hz]	flutter type
NASTRAN	5.39	11.4	15.2	11.3	14.9	α – torsion
FEM	5.38	11.5	15.0	11.1	14.92	

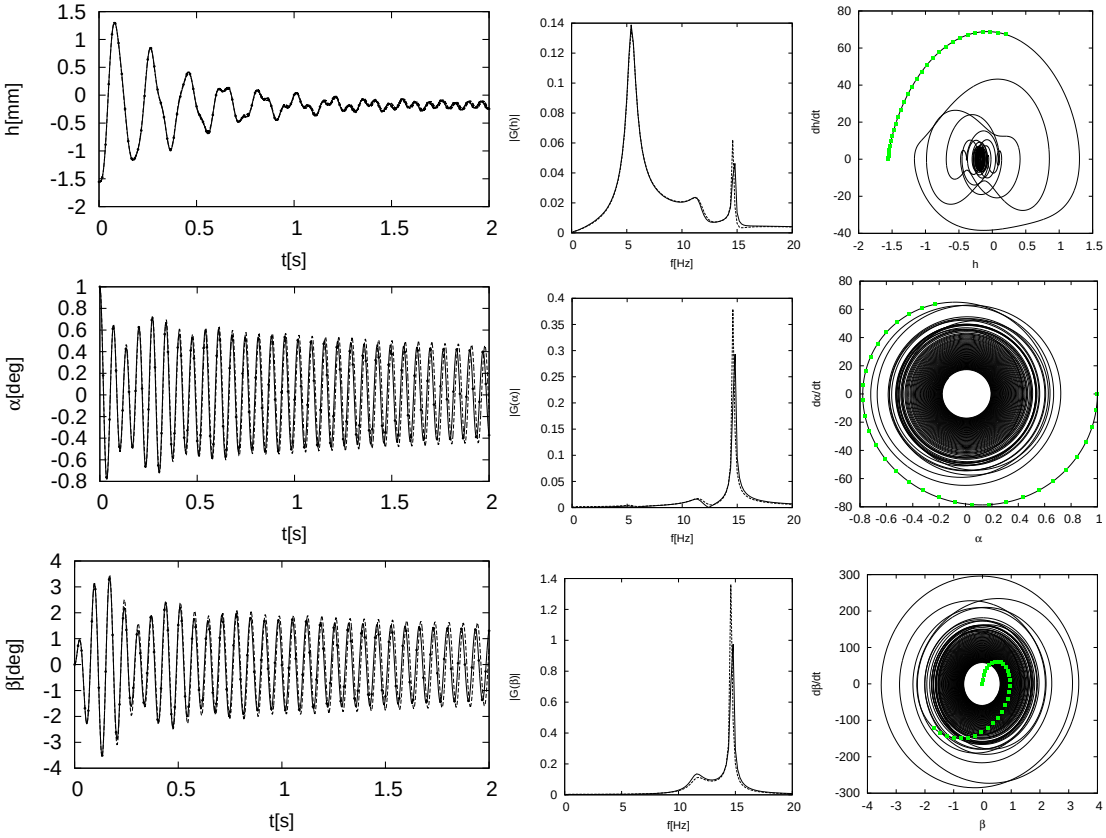

Figure 4: Airfoil with gap 0.54%: Functions $h(t)$, $\alpha(t)$, $\beta(t)$ (left), their spectra (middle) and phase diagrams (right) for $k-\omega$ (full line) and Spalart-Allmaras turbulence model (dashed line) and far-field airflow velocity 9 m/s.

by the $k-\omega$ turbulence model and the system is more stable comparing to the use of the Spalart-Allmaras model.

This behaviour is demonstrated in Fig. 9, which shows the damping ratio $D=\ln\frac{\alpha_0/\alpha_n}{2\pi n}$, calculated from n cycles of the time response of the airfoil for the rotation angle amplitudes α_0 and α_n, in dependence on the far-field air flow velocity for three different gaps.

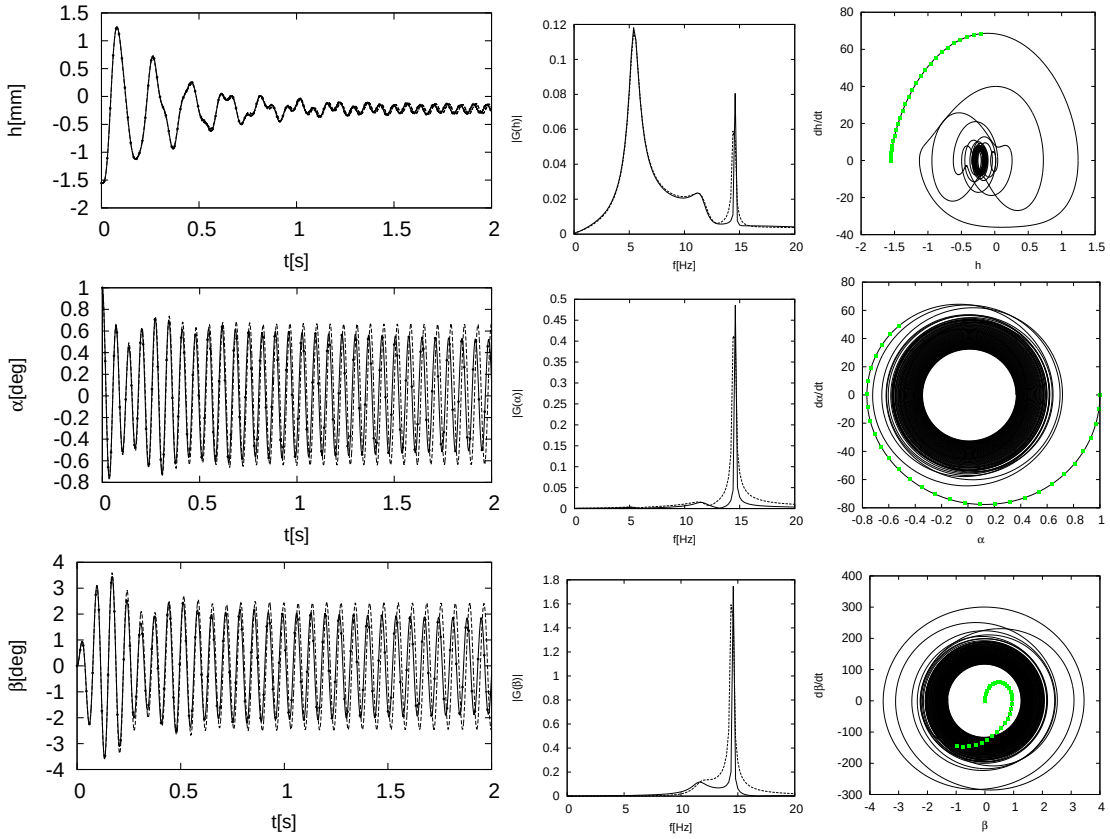

Figure 5: Airfoil with gap 0.54%: Functions $h(t)$, $\alpha(t)$, $\beta(t)$ (left), their spectra (middle) and phase diagrams (right) for $k-\omega$ (full line) and Spalart-Allmaras turbulence model (dashed line) and far-field airflow velocity 10 m/s.

If the damping ratio $D>0$, the system is stable, and when $D<0$, the system is unstable by coupled mode flutter for the rotations α and β. For example, for the gap width $g=3.74\%$ and the far-field air flow velocity 10 m/s the system is stable ($D>0$) when using the $k-\omega$ turbulence model and unstable ($D<0$) by flutter when the Spalart-Allmaras turbulence model is used.

The critical flutter velocities U_F evaluated from the damping ratio of the numerically simulated time signals are shown in Fig. 10 in dependence on the gap width between the airfoil and the flap. The flutter velocity $U_F \approx 11.1$ m/s computed for the smallest gap $g=$ 0.54% by using the $k-\omega$ turbulence model is in good agreement with the flutter velocity 11.32 m/s computed by NASTRAN (see [28] and [29]), where no gap was considered and the linear theory was used. The use of the Spalart Allmaras model in the numerical simulations results in the lower flutter velocities and by increasing the gap width the flutter velocities are getting lower. We should note here that for the gap shape considered (see Fig. 2) it is impossible to simulate properly the cases for zero or very narrow gaps due

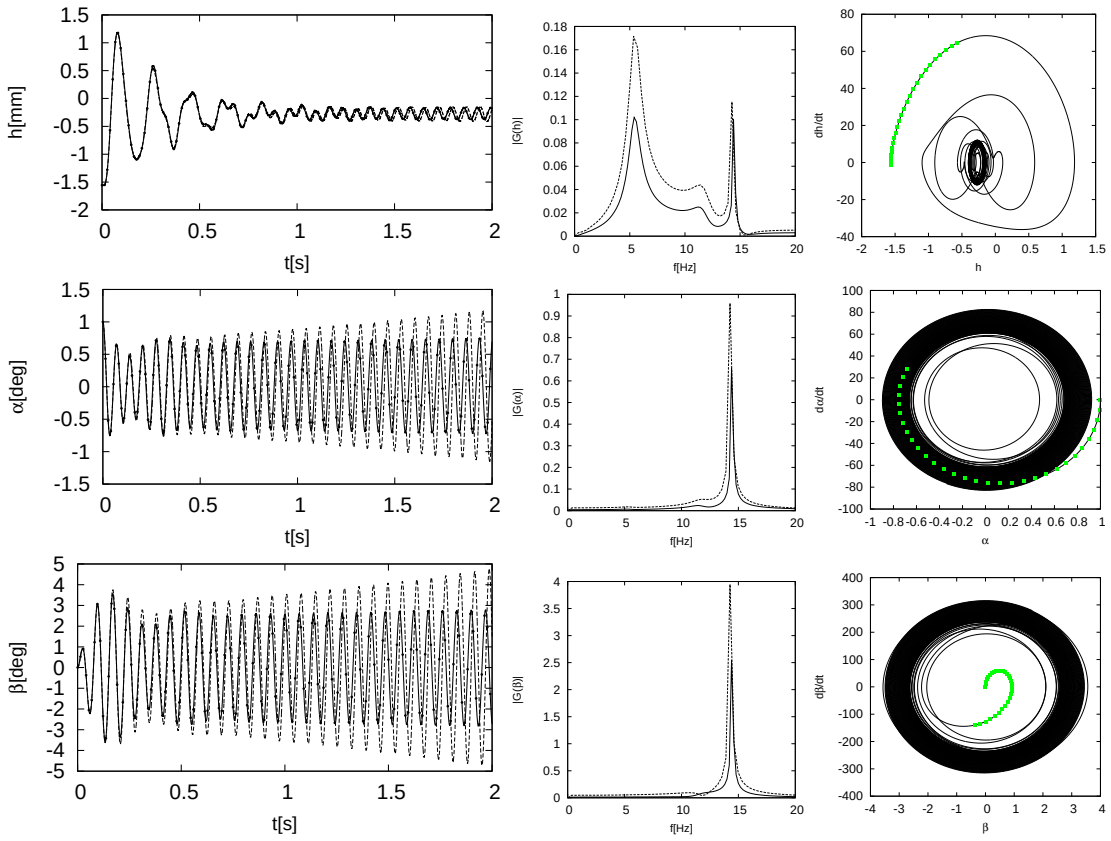

Figure 6: Airfoil with gap 0.54%: Functions $h(t)$, $\alpha(t)$, $\beta(t)$ (left), their spectra (middle) and phase diagrams (right) for $k-\omega$ (full line) and Spalart-Allmaras turbulence model (dashed line) and far-field airflow velocity 11 m/s.

to a technically limited maximum of the angle for the flap rotation and related meshing problems due to contacts of the moving profile and flap surfaces.

Comparison of the presented finite element method with MSC.NASTRAN computations is summarized in Table 1. It shows the vibration frequencies for all three displacements $h(t)$, $\alpha(t)$, $\beta(t)$ for a low far-field flow velocity and the critical flutter velocity together with the corresponding frequency computed by the presented finite element method, compared with the NASTRAN computations.

6.2 Numerical simulation of post flutter behaviour with large vibration amplitudes

Up to now, the vibration amplitudes in all examples presented did not exceed extremely high values as can be encountered for the far-field flow velocities higher than the flutter velocity. Such example is presented in Figs. 11-14 for the far-field velocity $U_\infty = 11$

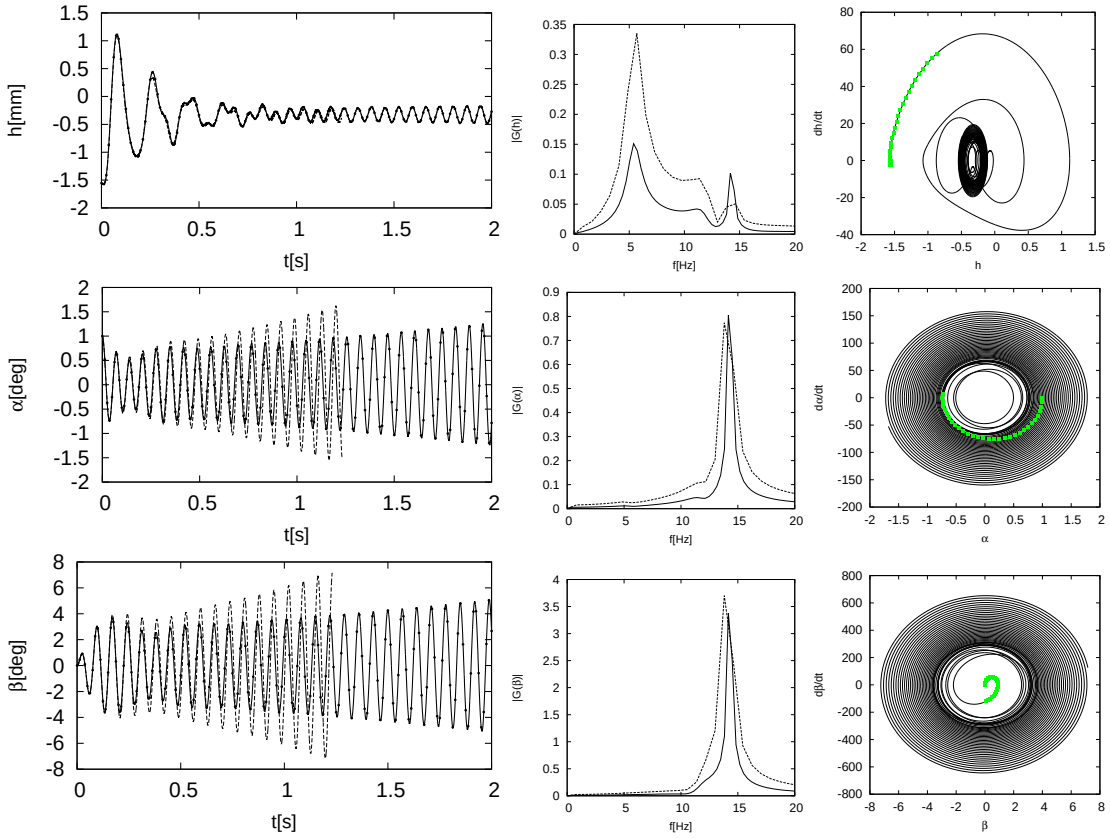

Figure 7: Airfoil with gap 0.54%: Functions $h(t)$, $\alpha(t)$, $\beta(t)$ (left), their spectra (middle) and phase diagrams (right) for $k-\omega$ (full line) and Spalart-Allmaras turbulence model (dashed line) and far-field airflow velocity 12 m/s.

m/s and the gap 6.95%. The vibration amplitude for the flap is growing up to nearly 40 degrees when the numerical simulation failed due to a large computational mesh deformation. The corresponding computed velocity flow fields around the fluttering airfoil are shown in Figs. 12-14 at several time instants marked in Fig. 11. The shown velocity is defined as the magnitude of the velocity related to the far-field velocity. It is possible to see clearly the flow separation on the flap surface, especially on the detailed snapshots viewing the velocity flow field around the flap.

7 Conclusion

The paper was concerned with the numerical solution of airfoil vibrations induced by turbulent flow. The motion of the airfoil with three degrees of freedom is described by a system of three second-order nonlinear ordinary differential equations for the vertical displacement and rotation angles of the main airfoil body and the flap. The flow is mod-

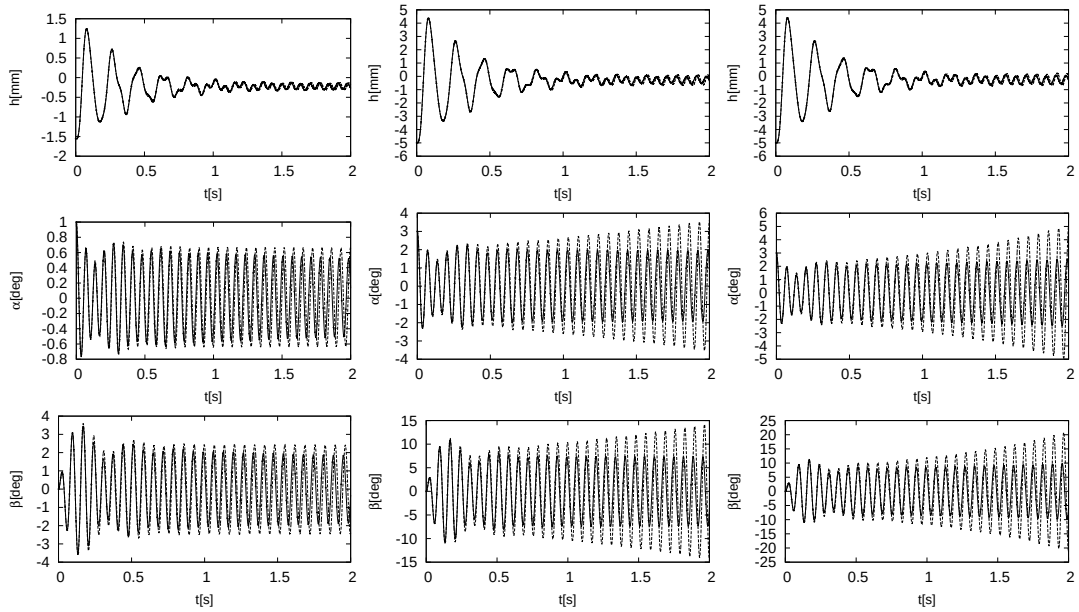

Figure 8: Functions $h(t)$, $\alpha(t)$, $\beta(t)$ computed by the Spalart-Allmaras (dashed line) and $k-\omega$ (solid line) turbulence models for the far-field velocity 10 m/s and the gaps: 0.54% (left), 3.74% (middle) and 5.58% (right).

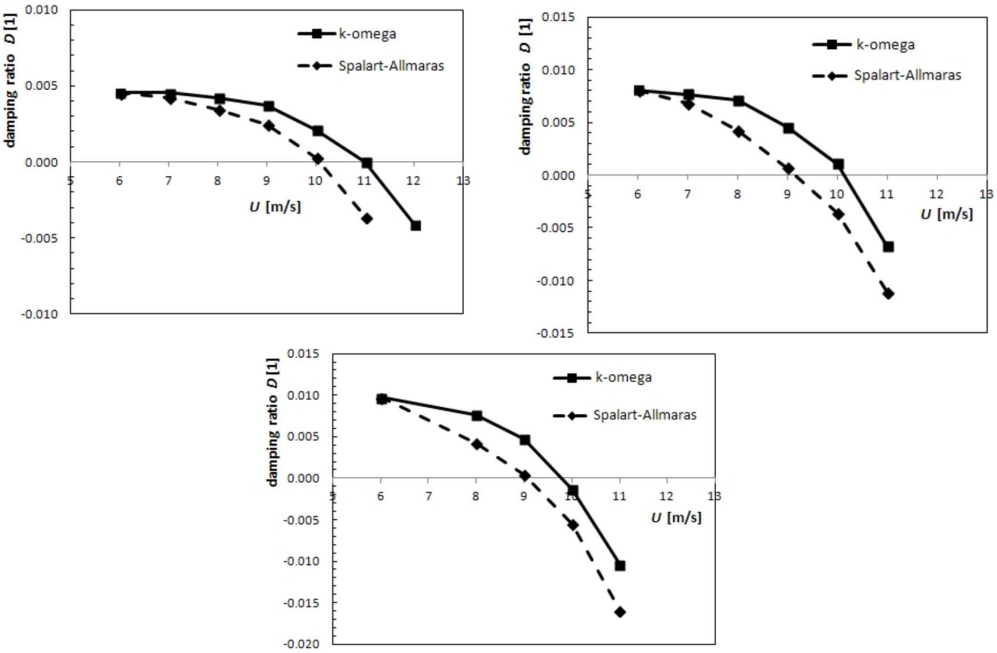

Figure 9: Aerodynamic damping versus far-field flow velocity for the gaps of the width 0.54%, 3.74% and 5.28%.

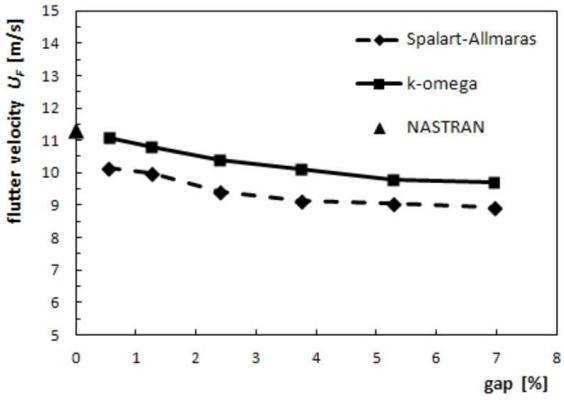

Figure 10: Flutter velocity computed by NASTRAN (Δ) and by the developed method using the Spalart-Allmaras (dashed line) or $k-\omega$ turbulence model (full line) in dependence on the gap between the airfoil and the flap.

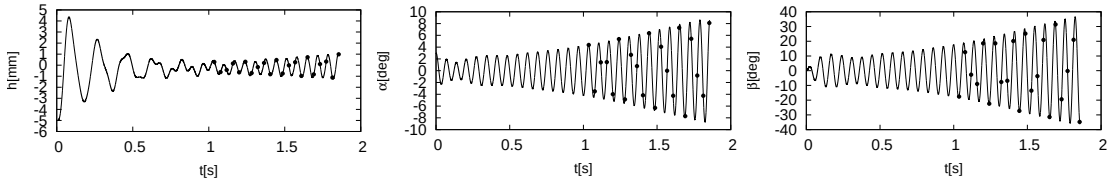

Figure 11: Functions $h(t)$, $\alpha(t)$, $\beta(t)$ computed by the $k-\omega$ model for $U_\infty=11$ m/s and the gap width 6.95%.

elled by the incompressible Reynolds averaged Navier-Stokes equations (RANS) with the Spalart-Allmaras and $k-\omega$ turbulence models.

The developed method is based on several important ingredients:

- second-order BDF time discretization and the space discretization by the FEM for the solution of the RANS system coupled with the partial differential equations describing the turbulence models,
- SUPG and div-div stabilization of the FEM for the RANS equations,
- SUPG and discontinuity capturing stabilizations of the FEM for the turbulence models,
- construction of the ALE mapping and the ALE velocity,
- algorithms for the realization of the solution of turbulent flow and of the fluid-structure interaction coupling.

Numerical experiments proved that the developed technique is robust with respect to the magnitude of the Reynolds number and allows the simulation of airfoil vibrations with large amplitudes.

The results of the numerical simulation show that the flutter stability boundary of the airfoil with three degrees of freedom can be sensitive to the gap width between the flap and the main airfoil lifting surface. This is caused by an interaction of the main airstream with the airflow through the gap. This aside flow influences the vortex shedding at the

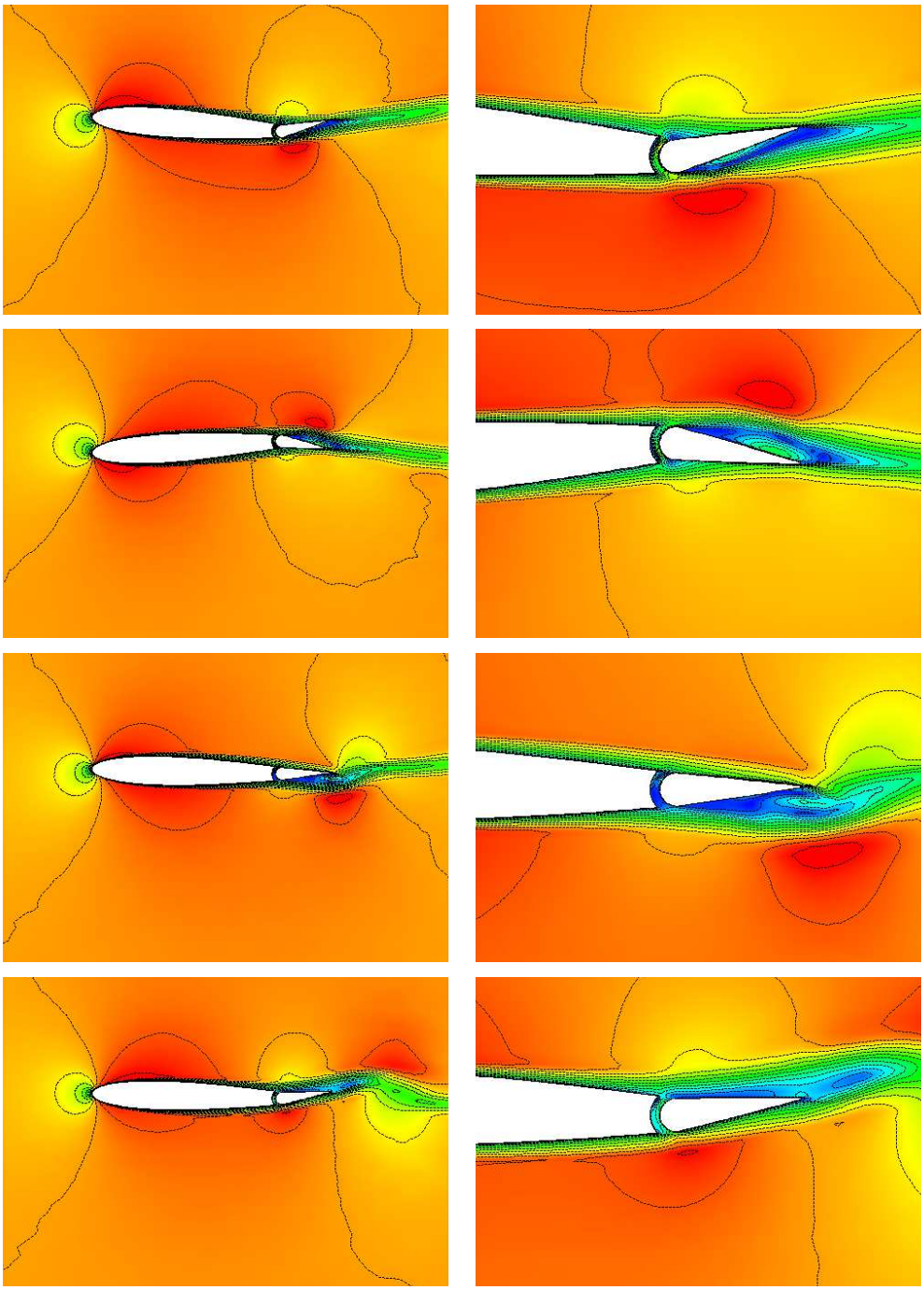

Figure 12: Velocity distribution around the fluttering profile for $U_\infty = 11$ m/s computed by the $k-\omega$ model at several time instants marked in Fig. 11 including a detail around the flap. Part I.

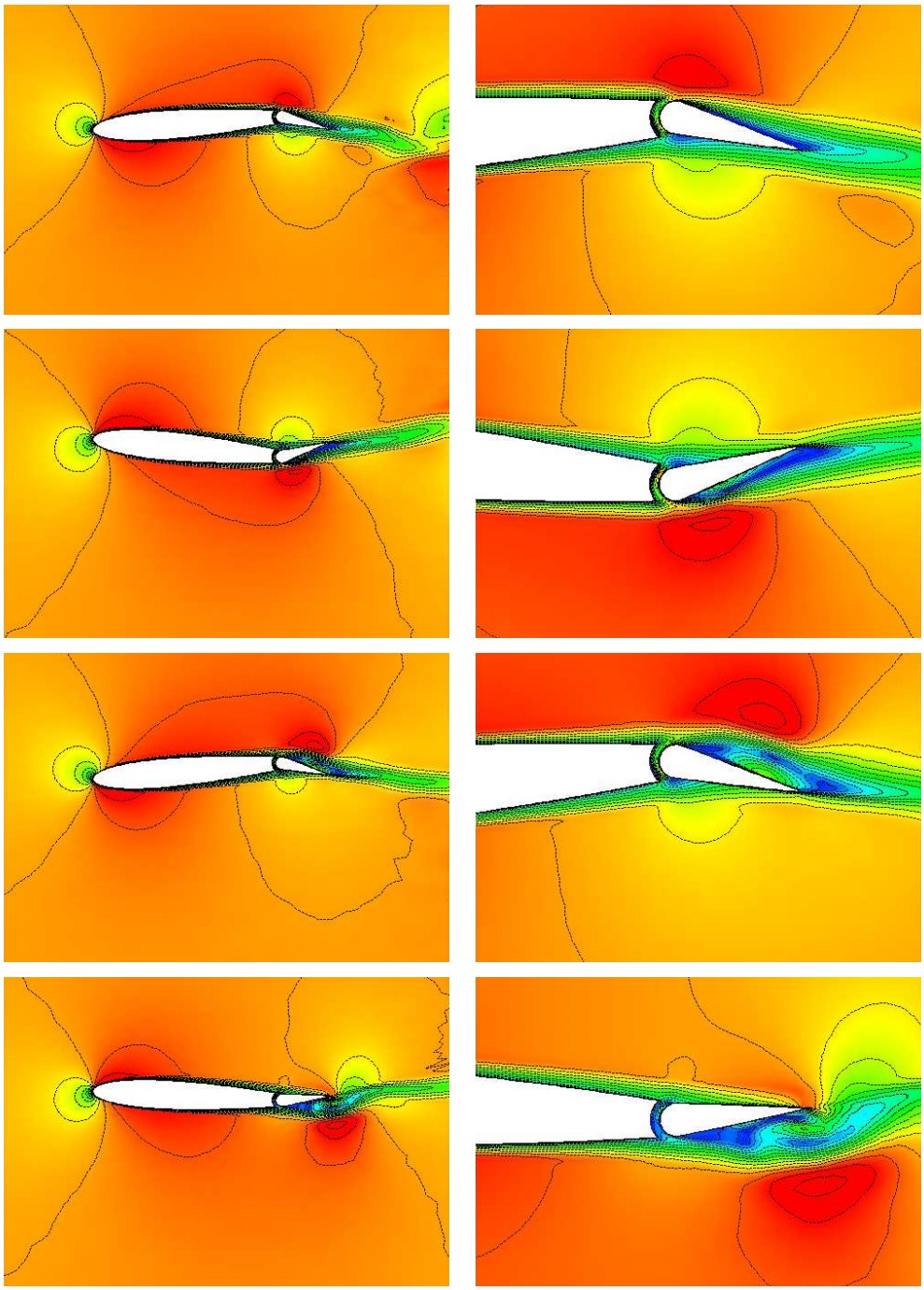

Figure 13: Velocity distribution around the fluttering profile for $U_\infty = 11$ m/s computed by the $k-\omega$ model at several time instants marked in Fig. 11 including a detail around the flap. Part II.

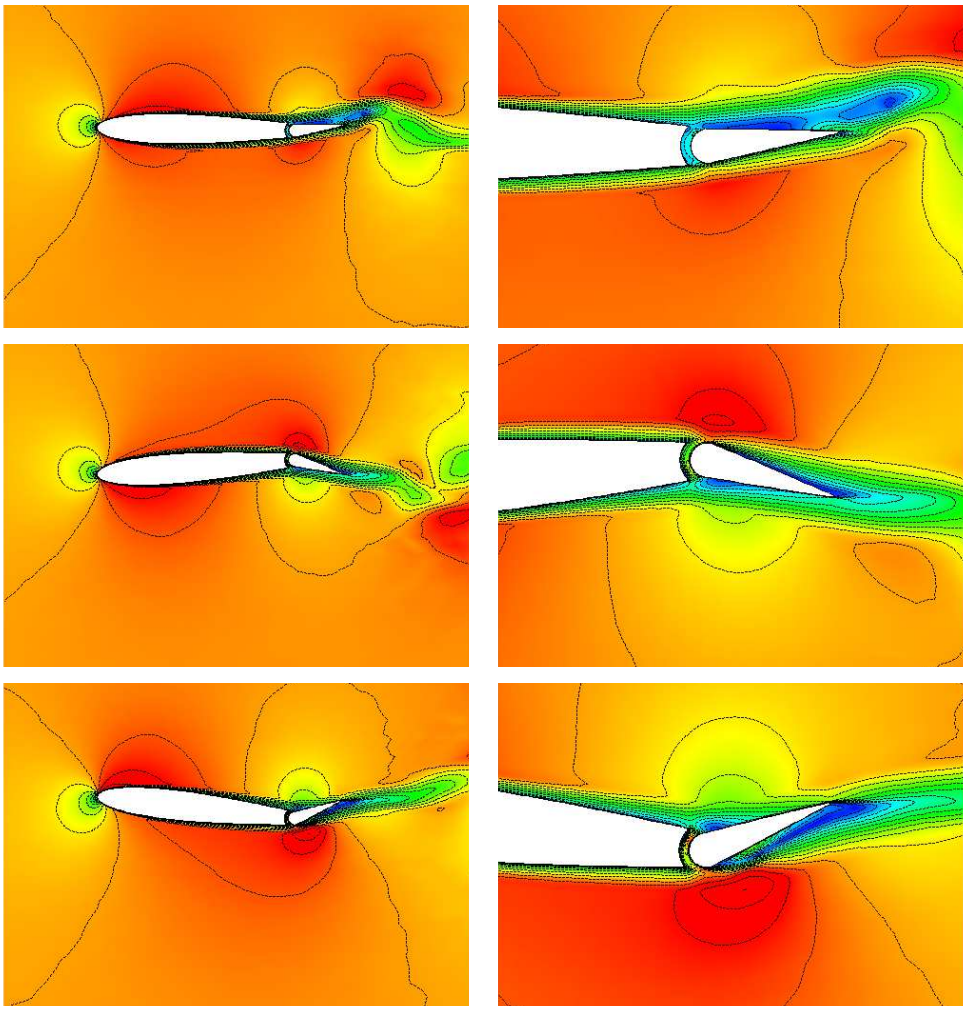

Figure 14: Velocity distribution around the fluttering profile for $U_\infty = 11$ m/s computed by the $k-\omega$ model at several time instants marked in Fig. 11 including a detail around the flap. Part III.

airfoil trailing edge, the limit cycle oscillation amplitudes and the critical flutter velocity. However, the results have to be accepted with a caution, because the critical flutter flow velocity of the system studied was very low and the influence of the flow inside the gap on the aeroelastic behavior of the airfoil can be reduced in cases of higher far-field airflow velocities.

The airflow transition to the turbulence on the profile surface as well as the flow separation is influenced by the airfoil vibration. The $k-\omega$ turbulence model corresponds better to the NASTRAN computation of the critical flutter velocity and this turbulence model seems better than the Spalart Allmaras model also for numerical simulation of the post flutter behavior of the system when the vibration amplitudes, especially for the flap rotation, are large.

There are several subjects of a further research:

- comparison of computational results with wind-tunnel experiments,
- increase of the speed of computational processes,
- extension to the numerical simulation of compressible flow,
- theoretical analysis of qualitative properties of the developed numerical technique.

Acknowledgments

This research was supported under the grants of the Czech Science Foundation No. P101/11/0207 (J. Horáček) and 13-00522S (M. Feistauer, P. Sváček).

References

[1] Badia S, Codina R (2007) On some fluid-structure iterative algorithms using pressure segregation methods. Application to aeroelesticity, Int. J. Numer. Meth. Engr. 72:46-71.
[2] Baxevanou CA, Chaviaropoulos PK, Voutsinas SG, Vlachos NS (2008) Evaluation study of a Navier-Stokes CFD aeroelastic model of wind turbine airfoils in classical flutter. J. Wind Engr. Ind. Aerod. 96:1425-1443.
[3] Brezzi F, Falk RS (1991) Stability of higher-order Hood-Taylor methods. SIAM J. Numer. Anal. 28:581-590.
[4] Brezzi F, Fortin M (1991) Mixed and Hybrid Finite Element Method. Springer Series in Computational Mathematics 15, Springer-Verlag, New York.
[5] Caracoglia L (2011) Simulation of linear and non-linear propagation effects of a random turbulence field on bridge flutter instability. J. Wind Engr. Ind. Aerod. 99(9):945-954.
[6] Ciarlet PG (1979) The Finite Element Method for Elliptic Problems. North-Holland, Amsterdam.
[7] Codina R (1993) A discontinuity capturing crosswind-dissipation for the finite element solution of the convection diffusion equation. Comput. Meth. Appl. Mech. Engr. 110:325342.
[8] Dolejší V (2001) ANGENER V3.0. Faculty of Mathematics and Physics, Charles University in Prague.
[9] Dolejší V (2001) Anisotropic mesh adaptation technique for viscous flow simulation. East-West J. Numer. Math. 9:1-24.
[10] Dowell EH (1995) A Modern Course in Aeroelasticity. Kluwer Academic Publishers, Dodrecht.
[11] Dubcová L, Feistauer M, Horáček J, Sváček P (2008) Numerical simulation of airfoil vibrations induced by turbulent flow. J. Comput. Appl. Math. 218(1):34-42.
[12] Dubcová L, Feistauer M, Horáček J, Sváček P (2009) Numerical simulation of interaction between turbulent flow and a vibrating airfoil. Comput. Visual. Sci. 12:207-225.
[13] Farhat C, Lesoinne M, Maman N (1995) Mixed explicit/implicit time integration of coupled aeroelastic problems: Three field formulation, geometric conservation and distributed solution. Int. J. Numer. Meth. Fluids 21:807-835.
[14] Feistauer M, Horáček J, Růžička M, Sváček P (2011) Numerical analysis of flow induced nonlinear vibrations of an airfoil with three degrees of freedom. Comput. Fluids 49:110-127.
[15] Foias C, Manley O, Rosa R, Temam R (2001) Navier-Stokes Equations and Turbulence. Cambridge University Press, Cambridge.

[16] Geissler W (2003) Numerical study of buffet and transonic flutter on the NLR 7301 airfoil. Aerosp. Sci. Tech. 7:540-550.
[17] Gelhard T, Lube G, Olshanskii MA, Starcke JH (2005) Stabilized finite element schemes with LBB-stable elements for incompressible flows. J. Comput. Appl. Math. 177:243-267.
[18] GMSH, http://www.geuz.org/gmsh.
[19] Geuzaine C, Remacle J F (2009) Gmsh: A three-dimensional finite element mesh generator with built-in pre- and post-processing facilities. Int. J. Numer. Meth. Engr. 79(11):1309-1331.
[20] Horáček J, Sváček P, Růžička M, Feistauer M (2007) Contribution to finite element modelling of airfoil aeroelastic instabilities. Appl. Comput. Mech. 1:43-52.
[21] John V, Knobloch P (2007) On spurious oscillations at layers diminishing (SOLD) method for convection-diffusion equations, Part I – A review. Comput. Meth. Appl. Mech. Engr. 196:2197-2215.
[22] Khadra K, Angot P, Parneix S, Caltarigone J-P (2000) Fictitious domain approach for numerical modelling of Navier-Stokes equations. Int. J. Numer. Meth. Fluids 34:651-684.
[23] Kok JC (1999) Resolving the dependence on free-stream values for the *k*-omega turbulence model, National Aerospace Laboratory, NLR Report p. 20.
[24] Langthjem MA, Morita H, Nakamura T, Nakano M (2006) A flexible rod in annular leakage flow: Influence of turbulence and equilibrium offset, and analysis of instability mechanisms. J. Fluids Struct. 22(5):617-645
[25] Le Tallec P, Mouro J (2001) Fluid structure interaction with large structural displacements. Comput. Meth. Appl. Mech. Engr. 190:3039-3067.
[26] Lian Y, Steen J, Trygg-Wilander M, Shyy W (2003) Low Reynolds number turbulent flows around a dynamically shaped airfoil. Comput. Fluids 32:287-303.
[27] Lojcjanskij LG (1978) Mechanics of Fluids and Gases. Nauka, Moscow (in Russian).
[28] Losík V, Čečrdle J (2005) Aeroelastic analysis of a verifying model of an airplane construction with three degrees of freedom – Part I. Research Report No. V-1833/3210/05, Aircraft Research and Test Institute (ARTI), Prague-Letňany, 22p. (in Czech).
[29] Losík V, Čečrdle J (2007) Flutter computation of 3-DOF wing profile model. Technical report P-PL-0061/07, Aircraft Research and Test Institute (ARTI), Prague-Letňany, 12p. (in Czech).
[30] Lube G (1994) Kowalski, Jan Krzysztof (ed.) et al., Numerical Analysis and Mathematical Modelling. Warszawa: Polish Academy of Sciences, Inst. of Mathematics, Banach Cent. Publ. 29:85-104.
[31] Mannini C, Šoda A, Schewe G (2010) Unsteady RANS modelling of flow past a rectangular cylinder: Investigation of Reynolds number effects. Comput. Fluids 39:1609-1624.
[32] Mannini C, Šoda A, Vo R, Schewe G (2010) Unsteady RANS simulations of flow around a bridge section. J. Wind Engr. Ind. Aerod. 98:742-753.
[33] Matsuzaki Y, Torii H (1990) Response characteristics of a two-dimensional wing subjected to turbulence near the flutter boundary. J. Sound Vib. 136(2):187-199.
[34] Naudasher E, Rockwell D (1994) Flow-Induced Vibrations. A.A. Balkema, Rotterdam.
[35] Nomura T, Hughes TJR (1992) An arbitrary Lagrangian-Eulerian finite element method for interaction of fluid and a rigid body, Comput. Meth. Appl. Mech. Engr. 95:115-138.
[36] Poirel DC, Price SJ (1996) Numerical investigation of the stability and post-flutter response of a 2D nonlinear airfoil in longitudinal atmospheric turbulence. Collection of Technical Papers – AIAA/ASME/ASCE/AHS/ASC Structures, Structural Dynamics and Materials Conference, 1:204-214.
[37] Poirel D, Price SJ (2003) Random binary (coalescence) flutter of a two-dimensional linear airfoil. J. Fluids Struct. 18:23-42.

[38] Poirel D, Price SJ (2007) Bifurcation characteristics of a two-dimensional structurally nonlinear airfoil in turbulent flow. Nonlinear Dynamics, 48(4):423-435.
[39] Poirel D, Métivier V, Dumas G (2011) Computational aeroelastic simulations of self-sustained pitch oscillations of a NACA0012 at transitional Reynolds numbers. J. Fluids Struct. 27:1262-1277.
[40] Pope SB (2000) Turbulent Flows. Cambridge University Press, Cambridge.
[41] Salvatori L, Spinelli P (2006) Effects of structural nonlinearity and along-span wind coherence on suspension bridge aerodynamics: Some numerical simulation results. J. Wind Engr. Ind. Aerod. 94(5):415-430.
[42] Schlichting H, Gersten K (2000) Boundary Layer Theory (8th edition). Springer, Berlin.
[43] Schlichting H, Gersten K (2006) Grenzschicht-Theorie (10th edition). Springer, Berlin.
[44] Spalart PR, Allmaras SR (1994) A one equation turbulence model for aerodynamic flows. Recherche Aérospatiale 1:5-21.
[45] Srinivasan GR, Ekaterinaris JA, Mc Croskey WJ (1995) Evaluation of turbulence models for unsteady flows of an oscillating airfoil. Comput. Fluids 24(7):833-861.
[46] Stanišić MM (1988) The Mathematical Theory of Turbulence. Springer, New York.
[47] Sváček P, Feistauer M, Horáček J (2007) Numerical simulation of flow induced airfoil vibrations with large amplitudes. J. Fluids Struct. 23:391-411.
[48] Taylor C, Hood P (1973) A numerical solution of the Navier-Stokes equations using the finite element technique. Comput. Fluids 1:73-100.
[49] Verfürth R (1984) Error estimates for a mixed finite element approximation of the Stokes equations. RAIRO, Anal. Numr. 18:175-182.
[50] Wang B, Zha GC (2011) Detached-eddy simulation of transonic limit cycle oscillations using high order schemes. Comput. Fluids 52:58-68.
[51] Weber S, Jones KD, Ekaterinaris JA, Platzer MF (2001) Transonic flutter computations for the NLR 7301 supercritical airfoil. Aerosp. Sci. Tech. 5:293-304.
[52] Wilcox DC (1993) Turbulence Modeling for CFD. DCW Industries, La Cañada, California.
[53] Zhao D, Zhang Q, Tan Y (2009) Random flutter of a 2-DOF nonlinear airfoil in pitch and plunge with freeplay in pitch. Nonlinear Dynamics 58(4):643-654.
[54] Zhao DM, Zhang QC, Wang W (2009) Random bifurcation and power spectrum analysis of a 2-DOF airfoil with freeplay nonlinearity in pitch. J. Vib. Shock 28(6):86-89.